REMI/HEAT COOL, a model for evaluation of core heat-up and emergency core spray cooling system performance for light-water-cooled nuclear power reactors

Munthe Andersen, J.G.

Publication date:
1973

Document Version
Publisher's PDF, also known as Version of record

Risø Report No. 296

Risø Report No. 296

Danish Atomic Energy Commission

Research Establishment Risø

REMI/HEAT COOL, A Model for Evaluation of Core Heat-Up and Emergency Core Spray Cooling System Performance for Light-Water-Cooled Nuclear Power Reactors

by Jens G. Munthe Andersen

September 1973

Sales distributors: Jul. Gjellerup, 87, Sølvgade, DK-1307 Copenhagen K, Denmark

Available on exchange from: Library, Danish Atomic Energy Commission, Risø, DK-4000 Roskilde, Denmark

September 1973 Risø Report No. 296

REMI/HEAT COOL, A Model for Evaluation of Core Heat-Up and Emergency Core Spray Cooling System Performance for Light-Water-Cooled Nuclear Power Reactors

by

Jens G. Munthe Andersen

Danish Atomic Energy Commission
Research Establishment Risø
Reactor Physics Department

Abstract

A description is given of a model for evaluation of core heat-up transients and the performance of emergency core spray cooling systems for light-water reactors. The model is based on a detailed analysis of the energy generation including metal-water reactions, heat conduction, forced convection, boiling heat transfer, thermal radiation, and the two-phase flow based on thermal non-equilibrium in the core and the primary system. The applicability of the model is demonstrated by comparison with the BWR-FLECHT experiments and a BWR/6 calculation.

This report is submitted to the Technical University of Denmark in partial fulfilment of the requirements for obtaining the lic. techn. (Ph. D.) degree.

UDC 621.039.588:681.3.06:519.283

INIS Descriptors

CHEMICAL REACTIONS
ECCS
DROPLETS
FORCED CONVECTION
FUEL RODS
LOSS OF COOLANT
MATHEMATICAL MODELS
NUCLEATE BOILING
POWER REACTORS
R CODES
RADIANT HEAT TRANSFER
REACTOR COOLING SYSTEMS
REACTOR SAFETY
SPRAYS
STEAM
THERMAL CONVECTION
TRANSIENTS
TWO-PHASE FLOW
WATER
WATER COOLED REACTORS
ZIRCALOY

ISBN 87 550 0222 6

CONTENTS

Page

1. Introduction 5
2. General Aspects of Reactor Safety and Accident Analysis 5
   - 2.1. Safety Criteria 6
   - 2.2. The Loss-of-Coolant Accident 7
   - 2.3. Emergency Core Cooling Systems 8
   - 2.4. RHC, a Model for Accident Analysis 8
3. The Mathematical Model 8
   - 3.1. The Geometrical Model 9
   - 3.2. Energy Generation Rates 9
     - 3.2.1. Decay of Fission Products and Actinides 9
     - 3.2.2. Metal-Water Reaction 10
   - 3.3. Heat and Mass Transfer 11
     - 3.3.1. Convective Heat Transfer to Superheated Steam . 11
     - 3.3.2. Heat Transfer between the Cladding or Shroud and a Falling Film 13
     - 3.3.3. Nucleate Boiling 15
     - 3.3.4. Heat and Mass Transfer at a Steam-Water Interface 16
     - 3.3.5. Thermal Radiation 18
       - 3.3.5.1. Calculation of the View Factors and the Beam Lengths 21
       - 3.3.5.2. Calculation of the Transmissivity 24
   - 3.4. Energy Balance for the Fuel 27
   - 3.5. Mass, Momentum, and Energy Balance for the Two-Phase Flow 29
     - 3.5.1. Film Flow 29
     - 3.5.2. Drop Flow 30
       - 3.5.2.1. The Spray System and the Droplet Production 31
       - 3.5.2.2. Drop Flow in the Primary System 36
     - 3.5.3. Steam Flow 38
   - 3.6. Thermodynamic Properties 42
   - 3.7. Computing Times 42

Page

4. BWR-FLECHT Calculations 43
4.1. Description of BWR-FLECHT Test Facility 43
4.2. Comparison of Experimental Data and RHC Calculations . 48
4.3. Conclusions from the BWR-FLECHT Calculations 64
5. BWR/6 Calculations 65
5.1. Description of the BWR/6-238 65
5.2. RHC Calculations on the BWR/6-238 71
5.3. Conclusions from the BWR/6 Calculations 78
6. Discussion and Conclusions 79
7. Acknowledgement 80
8. References 81
Appendix 84

1. INTRODUCTION

Accident analysis is an essential part of the safety analysis of a nuclear power reactor, and one of the main topics of this analysis is the loss-of-coolant accident (LOCA). A loss-of-coolant accident represents a risk of severe damage to the reactor as well as release of radioactivity.

An analysis of a LOCA involves a detailed investigation of the reliability of the system including the engineered safety system, the blow-down, the core heat-up and the emergency core cooling, the containment and the damage to the fuel, and the release and transport of fission products to the environment.

This report describes a sophisticated model, REMI/HEAT COOL (RHC), for analysis of the core heat-up transient and the performance of the emergency core spray cooling system. The model involves a detailed evaluation of the heat transfer and two-phase flow in a fuel element and the primary system during the core heat-up and emergency core cooling transient.

In order to examine the applicability of RHC for evaluation of core heat-up and emergency core cooling transients, the model was compared with the BWR-FLECHT experiments[10,11]. The comparison was favourable, and it is shown that RHC is able to predict both the temperatures and the rewetting times of the rods and the shroud. Furthermore as a demonstration of the capability of the model a core heat-up and emergency core cooling transient was calculated for a BWR/6-238 reactor[28], which is a 1250 MWe GE reactor.

As a result of these calculations it appeared that the model RHC is a powerful tool for evaluation of core heat-up transients and the performance of emergency core spray cooling systems as part of the safety analysis of a nuclear power reactor.

2. GENERAL ASPECTS OF REACTOR SAFETY AND ACCIDENT ANALYSIS

A nuclear power reactor represents, as well as other activities of man, a public risk, but the risk of a nuclear power reactor is in the low part of what is commonly accepted[3,4] for other activities, e.g. oil-fired plants and car driving. The limits for a nuclear power reactor are a political decision and will not be discussed in this paper, but different approaches to reactor safety criteria will be briefly discussed.

The public risk of a nuclear power reactor is mainly that of release of radioactivity, either continuous release during operation or accidental release of part of the radioactive inventory. This paper only deals with the

latter, namely accidents involving a potential for release of radioactivity, and, to be more specific, the loss-of-coolant accidents.

2.1. Safety Criteria

When a safety evaluation of a nuclear power reactor is performed, all credible accidents involving a risk of release of radioactivity to the environment have to be considered. For a given reactor and a specific site a relation between the radioactivity released and the consequences is normally well known, and what is to be investigated is thus the probability of a given accident and subsequent release of radioactivity. Once this analysis has been carried out, the results can be plotted in a diagram[1] as shown in fig. 2.1, which presents a typical safety criterion, a "Farmer curve", for

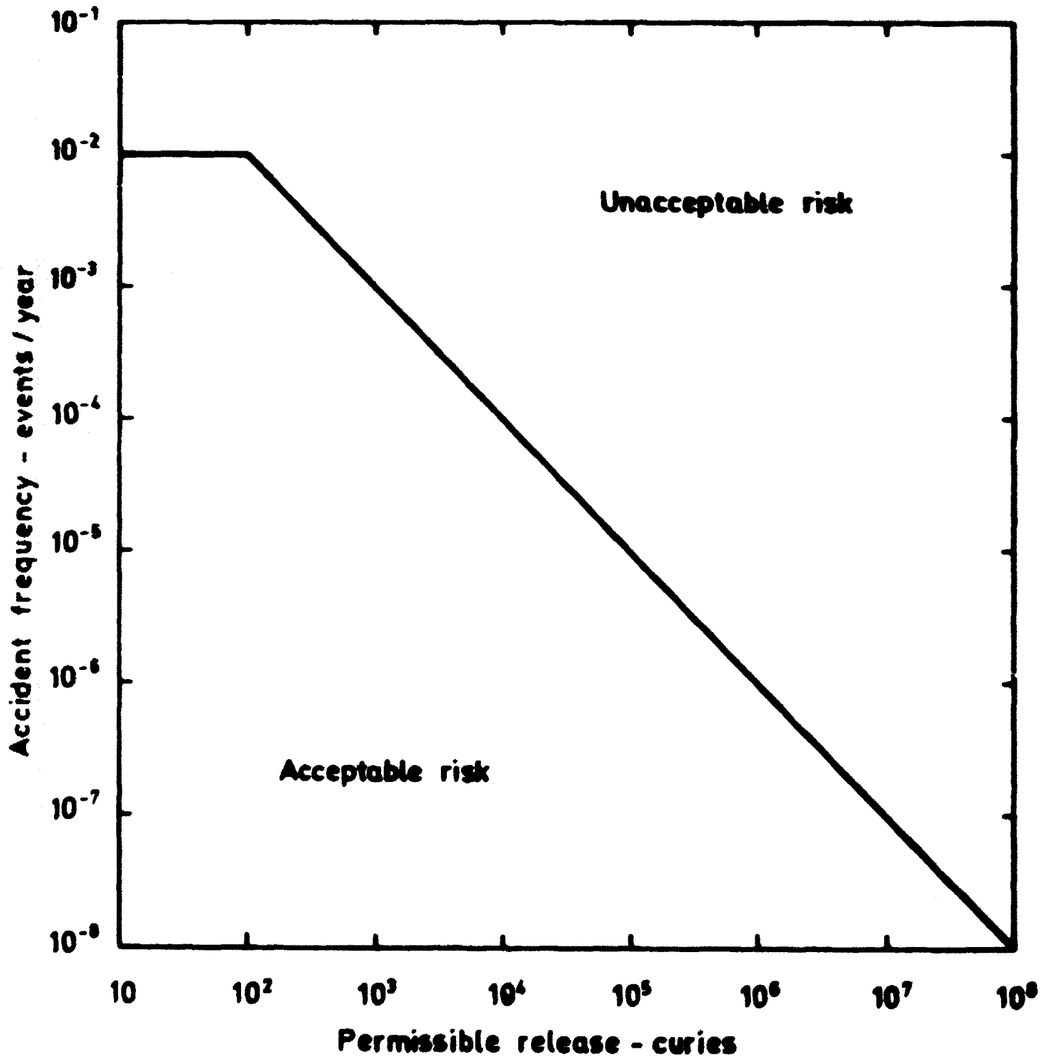

Fig. 2.1. Safety criterion.

a nuclear power reactor, and it can then be decided whether the safety is acceptable or not. However, some accidents have such severe environmental and economic consequences that they must be considered as unacceptable, and special safety criteria are made.

One of these serious accidents is a major loss-of-coolant accident, the design basis accident, which is a double-ended breach in one of the largest pipes connected to the reactor vessel. With respect to the design basis accident a special safety criterion is established[2] describing the reliability and capability of the engineered emergency core cooling system and the containment.

2.2. The Loss-of-Coolant Accident

After a breach in one of the major pipes connected to the vessel a blow-down will follow, and for a design basis accident the vessel will be emptied of water within 10-20 seconds. During this period burn-out will occur and the cladding temperature will begin to increase, mainly on account of a redistribution of the stored energy in the fuel. The nuclear chain reaction will cease very rapidly after the accident because of the increasing void during the blow-down, but owing to the decay of the fission products and of the actinides the energy production will continue for a long period of time at a level of the order of 5% of the power before the accident.

This will cause a further increase of the temperature, and within 100-200 seconds a temperature of 1200°C will be reached. At this temperature the chemical reaction between zirconium and steam becomes important, the temperature increase will accelerate, and after 50-100 seconds the cladding will start to melt at a temperature of 1850°C. The result is severe damage to the core and release of part of the volatile fission products. For example a typical light-water reactor contains in the order of 10^7-10^8 curies ^{131}I, and if the containment fails, a major part of this might be released to the environment.

These events are considered as unacceptable, and an emergency core cooling system able to prevent severe damage to the fuel and release of fission products is required. Furthermore a number of specifications as to the capability of the emergency core cooling system are set up[2]. But whether the criteria should consist of a number of rigorous demands on each single part of the engineered safety system, including the containment, or of a combined set of demands on the system as a whole, is an open question. The latter is more flexible and allows different optimizations, but requires much more as to the degree of sophistication in the safety analysis.

2.3. Emergency Core Cooling Systems

Two different emergency core cooling systems are generally used. One is a spray system normally placed above the core, but in a few cases it is an integrated part of the fuel elements, as e.g. in the SGHWR. The other is a flooding system. In BWR's both spray and flooding systems are used, whereas in PWR's only flooding systems are used. In either case the emergency core cooling system always consists of several independent systems.

With both spray and flooding systems heat is transferred from the hot fuel to the two-phase flow by convection and radiation, and the essential problem is to ensure that sufficient water is available to provide an effective heat sink. With spray systems the water will be found as a film flow on shroud and rods and as droplets between the rods. With flooding systems there is a water level in the vessel, and above this the liquid will be found as entrained droplets.

Owing to the close interaction between the heat transfer and the two-phase flow, an evaluation of the emergency core cooling system requires a rather sophisticated model for the physical phenomena involved.

2.4. RHC, a Model for Accident Analysis

In order to perform safety evaluations and accident analysis the model, REMI/HEAT COOL (RHC)[5], was developed for the physical phenomena involved in a loss-of-coolant accident. RHC is able to evaluate a core heat-up and emergency core spray cooling transient and perform a detailed analysis of the heat transfer and two-phase flow during the transient. Using suitable models for fuel rod failures and release and transport of fission products, the consequences of a postulated accident and the performance of the emergency core spray cooling system can be examined.

3. THE MATHEMATICAL MODEL

The model RHC is able to perform the calculation of a core heat-up transient under the influence of emergency core spray cooling for a single fuel element and a corresponding part of the primary circuit. The physical phenomena considered in the model are

1. The energy generation due to the decay of fission products and actinides, and the metal-water reaction.

2. Heat transfer due to thermal conduction in the fuel and the shroud, convection to the two-phase flow, and thermal radiation both from surface to surface and from surface to the two-phase flow.

3. The two-phase flow in the primary system, based on a separate description of the steam and water phase, and thermal non-equilibrium. The interchange of mass, momentum and energy between the phases is taken into account.

3.1. The Geometrical Model

The geometrical model consists of a single fuel element and a corresponding part of the primary system, represented as a closed loop (cf. fig. 3.1). The model of the primary system contains the lower plenum, the fuel element, upper plenum, riser and separator, steam dome, and downcomer. During the core heat-up transient the recirculation pumps have stopped, but a recirculation pump with locked impellers or a jet pump may be represented through their flow resistance. The breach may be anywhere in the downcomer between the lower plenum and the steam dome. Emergency core spray cooling water is introduced through nozzles situated in the upper plenum just under the riser.

3.2. Energy Generation Rates

The energy is generated by the decay of fission products and actinides, and the chemical metal-water reaction.

3.2.1. Decay of Fission Products and Actinides

The energy generation rate from the decay of fission products and of actinides is calculated by

$$Q_d = Q_o f(t) , \qquad (3.1)$$

where

Q_d is the decay heat, W/m^3,

Q_o the local power of the fuel at the time of the accident, W/m^3,

$f(t)$ the decay heat fraction, dimensionless, and

t the time since the accident, sec.

$f(t)$ is based on the history of the reactor before the accident and on the composition of the fuel. Normally $f(t)$ is based on the ANS-standard[6].

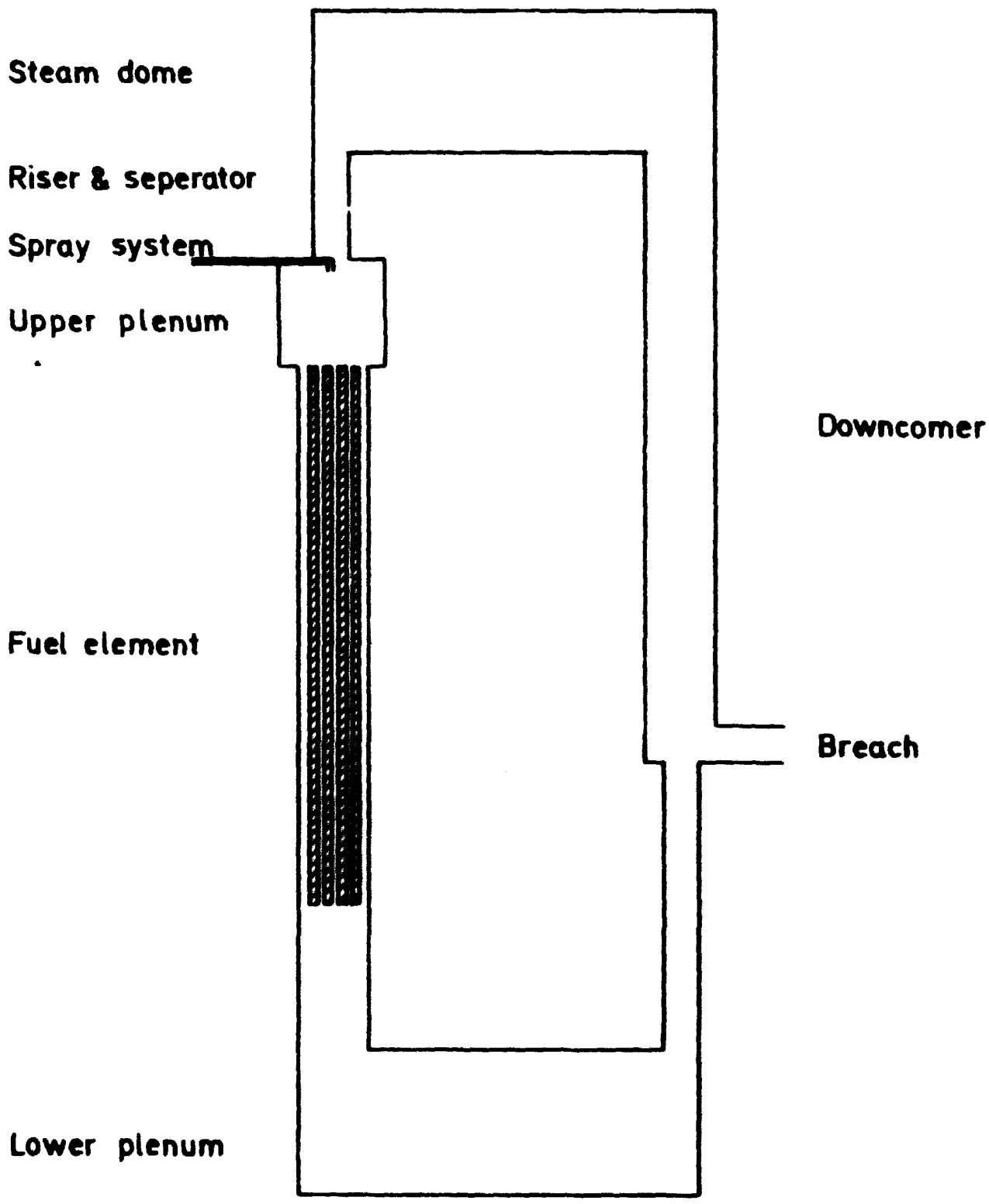

Fig. 3.1. The primary cirquit.

3.2.2. Metal-Water Reaction

At high temperatures Zr and steam will react chemically[7)]

$$Zr + 2H_2O \rightarrow ZrO_2 + 2H_2 + Q_M \qquad (3.2)$$

$$Q_M = 6.669 \cdot 10^6 - 0.257 \cdot 10^3 T_c, \qquad (3.3)$$

where

Q_M is the energy production, J/kg Zr, and

T_c the surface temperature, ^oC.

The reaction rate is determined by the diffusion of steam through the ZrO_2 layer at the surface, and a parabolic law exists

$$\frac{ds}{dt} = \frac{K}{s} \exp\left(\frac{-\Delta E}{R(T_c + 273.15)}\right), \qquad (3.4)$$

where

s is the thickness of the Zr layer converted into ZrO_2, m,

$K = 0.3937 \cdot 10^{-4}$ $m^2/sec.$,

$\Delta E = 1.905 \cdot 10^5$, the activation energy, J/mole, and

$R = 8.318$, the gas constant, J/mole ^oC.

In accordance with the USAEC Safety Criteria[2] the metal-water reaction is not assumed to be steam limited. However, this is only the case at very high temperatures and very little or no emergency core coolant, i.e. in the case of core melt-down, which is outside the scope of this model.

3.3. Heat and Mass Transfer

Heat is transferred from the fuel rods, the shroud, or any structural material to the two-phase flow in a number of different ways. Heat is transferred by forced convection from the fuel or the shroud to superheated steam near the surface or, if the surface is wetted by a falling film, to saturated or subcooled water. In the quench front of a falling film violent boiling will take place. Nucleate boiling will exist in the lower plenum owing to the large heat capacity of the vessel. Finally the intensity of thermal radiation in the fuel element is tremendous owing to the high surface temperatures, and a significant part of the radiation will be absorbed in the two-phase flow. The absorption of thermal radiation may be in a falling film on the shroud or a fuel rod, or in droplets between the rods.

3.3.1. Convective Heat Transfer to Superheated Steam

Convective heat transfer to superheated steam may take place either directly from the surface of the cladding or shroud, or, in the case of wetting by a falling film, from the film surface.

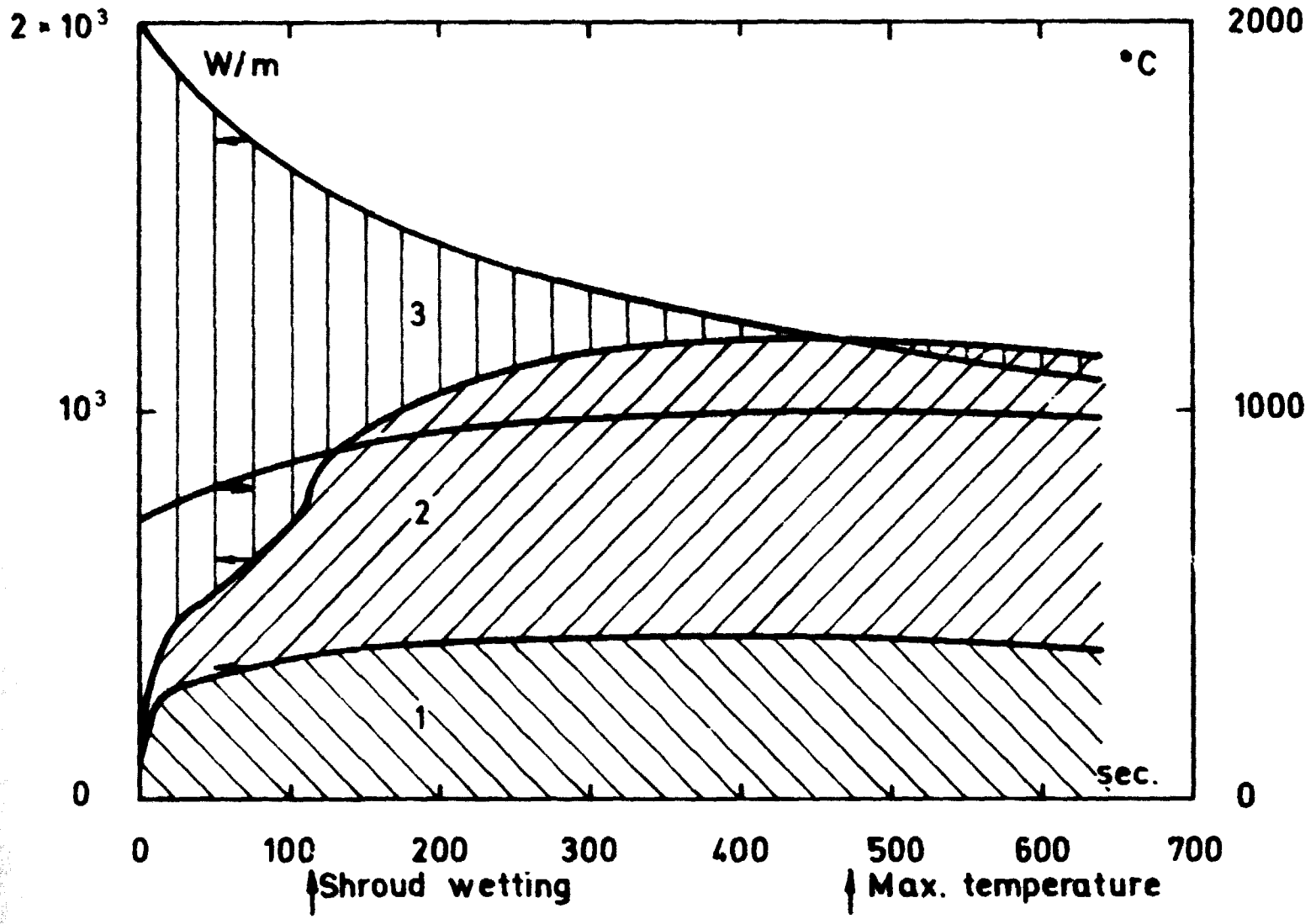

Fig. 3.2. Heat transfer and temperature for a BWR-FLECHT rod (group 2).

During the core heat-up transient the steam flow (cf. fig. 3.3) is most likely to be in the laminar flow region or in the lower part of the transition region and the Reynolds number will be smaller than 3000. For two reasons the flow is considered everywhere to be laminar, first, while the heat transfer in the transition regime is the largest, the assumptions of laminar flow will be conservative, and second, no common heat transfer correlation is known for the transition regime. This assumption implies (cf. chapter 4) that at high pressure, where thermal non-equilibrium is less marked, the model will tend to overpredict the cladding temperature.

For laminar flow the heat transfer for a constant heat flux is determined by [8]

$$Nu = \frac{hD_e}{k_g} = 3.316 + 0.895 \frac{s}{d}, \qquad (3.5)$$

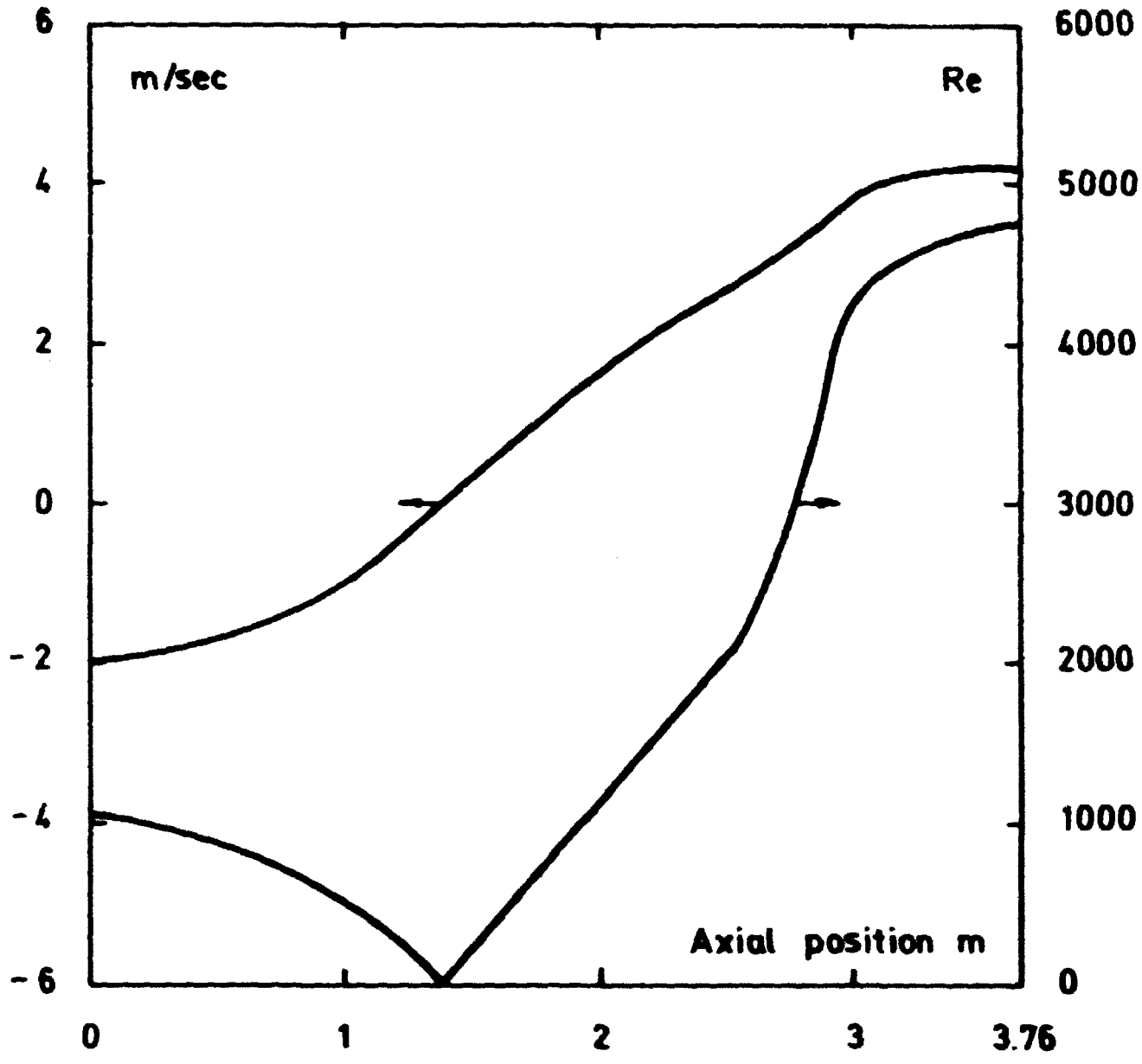

Fig. 3.3. Steam flow in a BWR/6 fuel element at time of maximum temperature, t = 350 seconds.

where

Nu is Nusselt's number, dimensionless,

h the heat transfer coefficient, $W/m^2\ ^oC$,

D_e the hydraulic diameter, m,

k_g the conductivity of steam, $W/m\ ^oC$,

s the pitch of the fuel rods, m, and

d the diameter of the fuel rods, m.

3.3.2. Heat Transfer between the Cladding or Shroud and a Falling Film

Heat will be transferred in two different ways to the falling film:

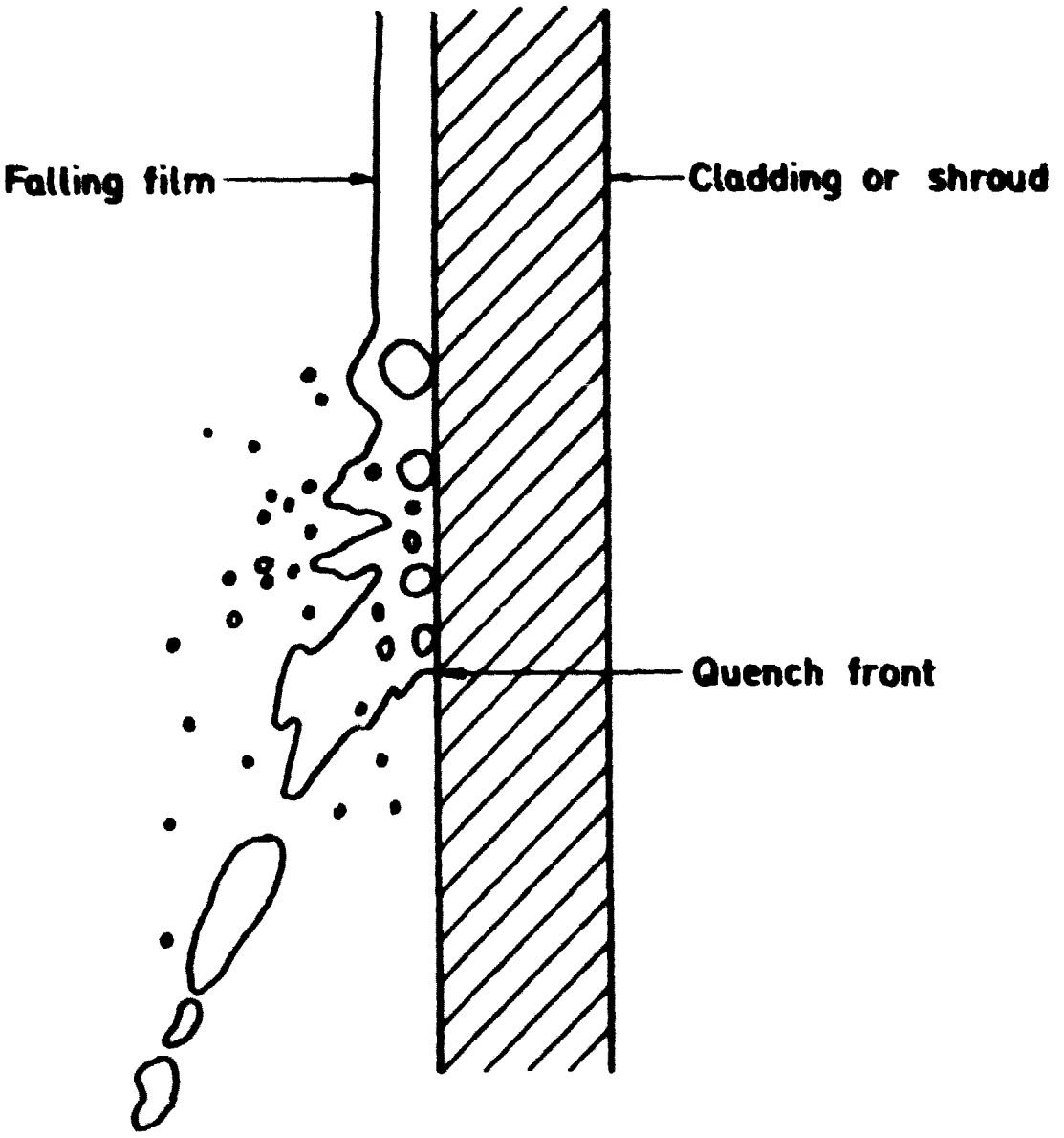

Fig. 3.4. Physical phenomena in rewetting.

At the film front there will be violent boiling, and upstream of the front the heat will be transferred by convection.

The heat transfer at the film front and the movement of the film front are determined by the material parameters of the wall, the temperature distribution in the wall, and the heat transfer coefficient to the film[9,19,22].

$$u_{fr} = \frac{1}{\rho_w c_w}\sqrt{\frac{h_{fr} k_w}{\delta_w}}\sqrt{\frac{(T_o - T_s)^2}{(T_\infty - T_s)(T_\infty - T_o)}} \qquad (3.6)$$

$$h_{fr} = 3.2 \cdot 10^6 \qquad (3.7)$$

$$T_o = \frac{1}{9.0945 \cdot 10^{-3} + \frac{3.6963 \cdot 10^3}{P}}, \qquad (3.8)$$

where

u_{fr} is the velocity of the film front, m/sec.,

ρ_w the density of the wall, kg/m^3,

c_w the heat capacity of the wall, J/kg ^oC,

h_{fr} the heat transfer coefficient at the front[10,11), $W/m^2\ ^oC$,

k_w the thermal conductivity of the wall, W/m ^oC,

δ_w the thickness of the wall, m,

T_o the Leidenfrost temperature[25, 26, 27), ^oC,

T_s the saturation temperature, ^oC,

T_∞ the temperature downstream of the front, ^oC, and

P the pressure, N/m^2.

The net heat transfer to the film front is now easily calculated

$$Q_{fr} = \delta_w \rho_w c_w (T_\infty - T_s) u_{fr}$$

$$= \left\{ \delta_w h_{fr} k_w \frac{T_\infty - T_s}{T_\infty - T_o} \right\}^{0.5} (T_o - T_s), \qquad (3.9)$$

where

Q_{fr} is the heat transfer at the film front, W/m.

Upstream of the film front a constant heat transfer coefficient[10,11) is used

$$h_f = 3.0 \cdot 10^3 - 5.0 \cdot 10^3\ W/m^2\ ^oC. \qquad (3.10)$$

3.3.3. Nucleate Boiling

After the blow-down some water will remain in the lower plenum, and owing to the large heat capacity of the vessel it will boil. The Rohsenow[12) correlation is used

$$\frac{c_l(T_w - T_s)}{H_{lg}} = 0.013 \left\{ \frac{Q_p}{\mu_l H_{lg}} \sqrt{\frac{\sigma}{g(\rho_l - \rho_g)}} \right\}^{0.33} Pr_l^{1.7}, \qquad (3.11)$$

where

c_l is the heat capacity of water, J/kg ^oC,

T_w the wall temperature, ^oC,

T_s the saturation temperature, ^oC,

H_{lg} the evaporation heat, J/kg,

Q_p the pool boiling heat transfer, W/m^2,

μ_l the viscosity of water, kg/m sec.,

σ the surface tension, N/m,

g = 9.81, the acceleration of gravity, $m/sec.^2$,

ρ_l the density of water, kg/m^3,

ρ_g the density of steam, kg/m^3, and

Pr_l Prandtl's number for water, dimensionless.

3.3.4. Heat and Mass Transfer at a Steam-Water Interface

Assuming that the steam-water interface has the saturation temperature, heat will be transferred to either side of the interface, and evaporation or condensation will take place.

Energy cannot be accumulated or lost at the interface, so if there is a difference between the heat transfer rates at the two sides, evaporation or condensation must take place at the interface.

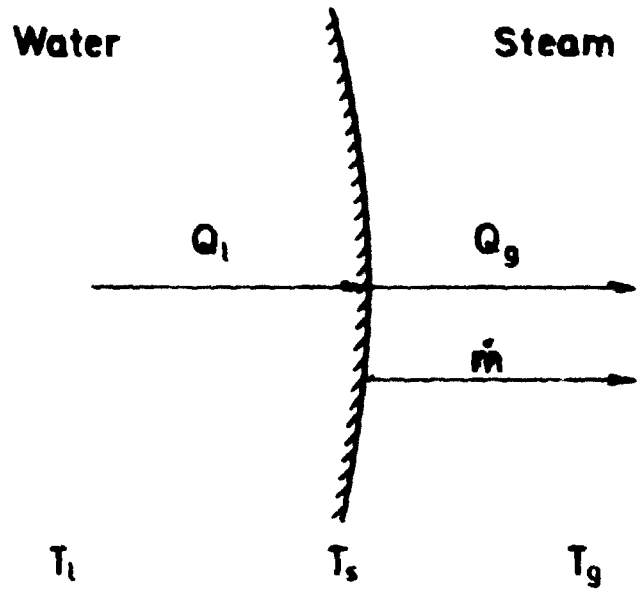

Fig. 3.5. Heat and mass transfer at a steam-water interface.

$$Q_l - Q_g = \dot{m} H_{lg}, \tag{3.12}$$

where

Q_l is the heat transfer from the water to the interface, W/m^2,

Q_g the heat transfer from the interface to the steam, W/m^2,

$\dot{m}$ the evaporation or condensation, $\dot{m}$ is positive for evaporation and negative for condensation, kg/m^2 sec.,

H_{lg} the evaporation heat, J/kg,

T_l the bulk temperature of water, ^oC,

T_s the saturation temperature, ^oC, and

T_g the bulk temperature of steam, ^oC.

If the interface is the interface between a film and steam, Q_g is determined by equation 3.5 and Q_l is given by

$$Q_l = \frac{2k_l}{s_f} (T_l - T_s), \tag{3.13}$$

where

k_l is the thermal conductivity of water, W/m ^oC, and

s_f the film thickness, m.

If the interface is the interface between a droplet and steam, φ_g is determined by[13)]

$$Nu = \frac{hd_d}{k_g} = 3.20 + 0.75\, Re_d^{0.5}\, Pr_g^{0.33} \tag{3.14}$$

$$Re_d = \frac{d_d \rho_g |u_g - u_d|}{\mu_g}\ , \tag{3.15}$$

where

Nu is Nusselt's number, dimensionless,

h the heat transfer coefficient, $W/m^2\,{}^oC$,

d_d the droplet diameter, m,

k_g the thermal conductivity of steam, $W/m\,{}^oC$,

Re_d Reynolds' number for the droplet, dimensionless,

Pr_g Prandtl's number for steam, dimensionless,

ρ_g the density of steam, kg/m^3,

u_g the velocity of steam, m/sec.,

u_d the velocity of the droplet, m/sec., and

μ_g the viscosity of steam, kg/m sec.

Q_l (cf. the Appendix) is determined by

$$Q_l = \frac{2}{3}\pi^2 \frac{k_l}{d_d}(T_l - T_s). \tag{3.16}$$

3.3.5. Thermal Radiation

Owing to thermal radiation energy will be transferred, both from surface to surface and from surface to the two-phase flow. Exchange of thermal radiation with the two-phase flow will mainly consist of absorption of radiation in the two-phase flow. On account of the relatively low temperature of the two-phase flow emission of thermal radiation is negligible.

The analytical model is based on the following assumptions:

1. All surfaces emit radiation uniformly.
2. All surfaces are grey and diffuse.
3. The medium between the surface is absorbing, but non-scattering and non-radiating.

4. Radiation in the axial direction is negligible.
5. The surfaces are in thermal equilibrium during each time step.

For a surface the radiosity is given by[14)]

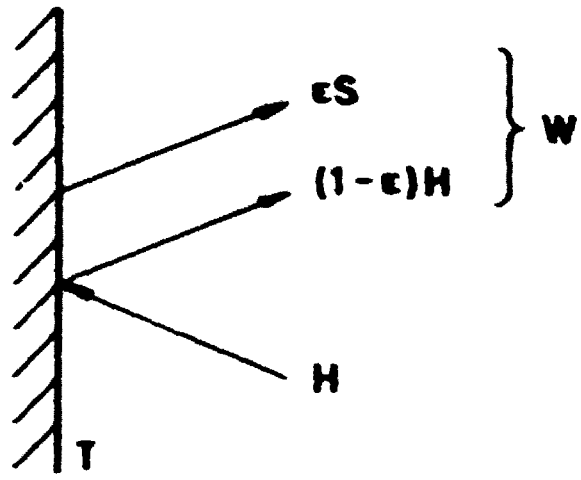

Fig. 3.6. Radiosity of a surface.

$$W = \varepsilon S + (1 - \varepsilon)H \qquad (3.17)$$

$$S = \sigma T^4, \qquad (3.18)$$

where

W is the radiosity, W/m^2,

ε the emissivity, dimensionless,

σ $= 5.6697 \cdot 10^{-8}$ is Stefan-Boltzmann's constant, $W/m^2\,{}^oK^4$,

T the surface temperature, ^oK, and

H the incoming radiation, W/m^2.

The first term on the right of (3.17) represents the radiation emitted by the surface, while the second represents the reflected radiation.

An energy balance for all surfaces and the medium between the surfaces gives

$$W_i = \varepsilon_i S_i + (1 - \varepsilon_i)H_i \qquad 1 \le i \le N \qquad (3.19)$$

$$A_i H_i = \sum_{j=1}^{j=N} A_j W_j F_{j,i} \tau_{j,i} \qquad 1 \le i \le N, \qquad (3.20)$$

where

$F_{i,j}$ is the view factor, dimensionless,

$\tau_{j,i}$ the transmissivity, dimensionless,

A_i the surface area, m^2,

the subscript "i" denotes the i'th surface, and

N the number of surfaces.

For the view factors and the transmissivities the following relations apply

$$\sum_{i=1}^{i=N} F_{j,i} = 1 \qquad 1 \leq j \leq N, \qquad (3.21)$$

$$0 \leq \tau_{j,i} \leq 1 \qquad 1 \leq j \leq N,\ 1 \leq i \leq N. \qquad (3.22)$$

If no radiation is absorbed in the two-phase flow, $\tau_{j,i} = 1$. Equations 3.19 and 3.20 may be rewritten to

$$\sum_{j=1}^{j=N} W_j(\delta_{j,i}A_i - (1 - \epsilon_i)A_jF_{j,i}\tau_{j,i}) = \epsilon_iS_iA_i \qquad 1 \leq i \leq N, \qquad (3.23)$$

where

$\delta_{j,i}$ is the Kronecker delta.

The view factors are dependent on the geometry only, and the transmissivities are dependent on the geometry, and the concentration, distribution, and spectrum of the droplets, and once they have been determined, equation 3.23 can be solved.

The net loss of energy from surface i is given by

$$Q_i = A_i(W_i - H_i), \qquad (3.24)$$

where

Q_i is the total loss of energy from surface i, W.

Combining equations 3.19 and 3.24 we obtain

$$Q_i = A_i \frac{\epsilon_i}{1 - \epsilon_i}(S_i - W_i). \qquad (3.25)$$

The rate at which energy is absorbed in the two-phase flow is equal to the net loss of energy from all the surfaces

$$Q_{abs} = \sum_{i=1}^{i=N} Q_i \,, \tag{3.26}$$

where

Q_{abs} is the total amount of energy absorbed, W.

Using equations 3.25, 3.19, and 3.20 in equation 3.26 we obtain

$$Q_{abs} = \sum_{i=1}^{i=N} \varepsilon_i \left(A_i S_i - \sum_{j=1}^{j=N} A_j W_j F_{j,i}\, \tau_{j,i}\right) . \tag{3.27}$$

And from the relations (3.21) and (3.22) it is seen that

$$0 \leq Q_{abs} \leq \sum_{i=1} A_i\, \varepsilon_i S_i \,, \tag{3.28}$$

which is self-evident, the lower boundary corresponds to $\tau_{i,j} = 0$, and the upper boundary to $\tau_{i,j} = 1$.

3.3.5.1. Calculation of the View Factors and the Beam Lengths

The view factors and beam lengths are dependent only on the geometry. Between two surfaces[14], the view factor is given by (cf. fig. 3.7)

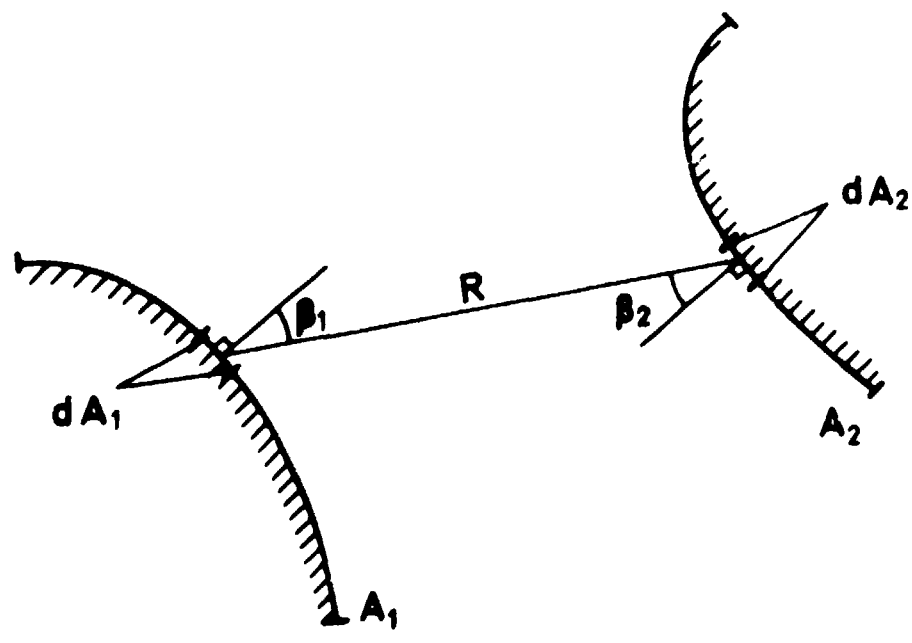

Fig. 3.7. Radiation heat transfer between two surfaces.

$$F_{1,2} = \frac{\int_{A_1}\int_{A_2} \frac{\cos\beta_1 \cos\beta_2}{\pi R^2} dA_2 dA_1}{\int_{A_1} dA_1} , \tag{3.29}$$

where

A is the surface area, m^2,

R the distance between the surfaces, m, and

β the angle between the normal and the beam, dimensionless.

The beam length is defined as the mean distance

$$R_{1,2} = \frac{\int_{A_1}\int_{A_2} \frac{\cos\beta_1 \cos\beta_2}{\pi R} dA_2 dA_1}{F_{1,2} A_1} . \tag{3.30}$$

From equations 3.29 and 3.30 it is seen that

$$A_1 F_{1,2} = A_2 F_{2,1} \tag{3.31}$$

$$R_{1,2} = R_{2,1} . \tag{3.32}$$

The view factors and the beam lengths are evaluated for a fuel element divided into a number of surfaces as shown in fig. 3.8. However, only the view factors are calculated exactly, for the beam lengths are used different approximations to equation 3.30.

For many applications different rods may be grouped together and treated identically, the shroud is normally treated as one surface (as it must be in this model). Let $i_1, i_2, \ldots, i_k$ be group i and $j_1, j_2, \ldots, j_l$ be group j; the reduced view factor $Fr_{i,j}$ and beam length $Rr_{i,j}$ between groups i and j are then in agreement with equations 3.29 and 3.30 given by

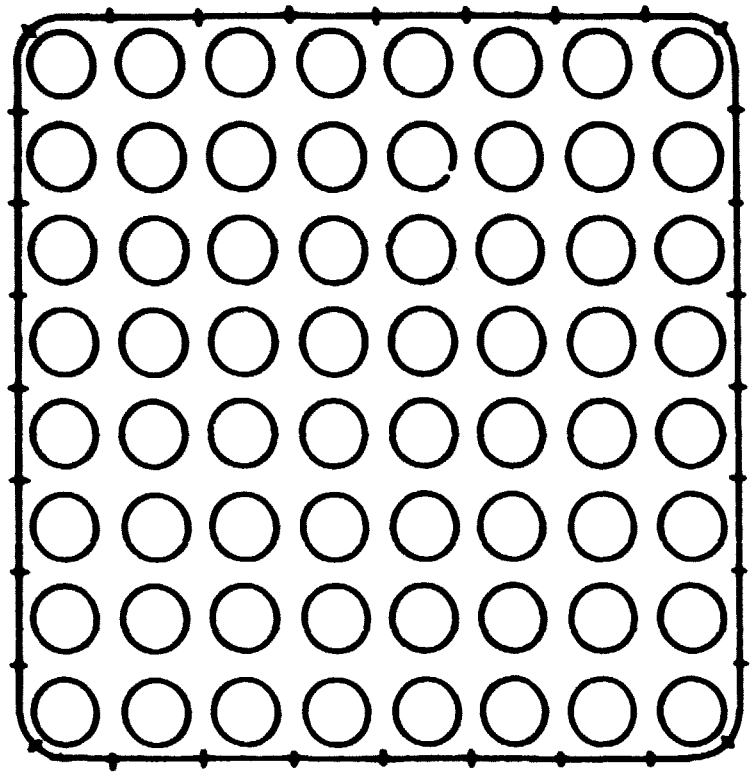

Fig. 3.8. Surfaces in a fuel element.

$$Fr_{i,j} = \frac{\sum_{m=i_k}^{m=i_l} \sum_{n=j_1}^{n=j_l} A_m F_{m,n}}{\sum_{m=i_1}^{m=i_k} A_m} , \qquad (3.33)$$

$$Rr_{i,j} = \frac{\sum_{m=i_k}^{m=i_l} \sum_{n=j_1}^{n=j_l} A_m F_{m,n} R_{m,n}}{Fr_{i,j} \sum_{m=i_1}^{m=i_k} A_m} , \qquad (3.34)$$

where

$Fr_{i,j}$ is the view factor between group i and group j, dimensionless,

and $Rr_{i,j}$ the beam length between group i and group j, m.

3.3.5.2. Calculation of the Transmissivity

In an absorbing medium a beam will be damped, and the damping is dependent on the absorption coefficient of the medium and the beam length

$$\frac{dI}{dx} = -\sigma(x)I \quad \langle = \rangle \tag{3.35}$$

$$I(x) = I(0) \exp\left\{-\int_0^x \sigma(t)dt\right\}, \tag{3.36}$$

where

I is the intensity of the beam, W/m^2,

x the length, m, and

σ the absorption coefficient, m^{-1}.

The absorption is based on the following assumptions:

1. Only the droplets absorb energy.
2. The droplets neither scatter nor emit radiation.
3. Only the fraction ε_l, where ε_l is the emissivity of the water, of the radiation hitting a droplet is absorbed, the rest $(1 - \varepsilon_l)$ is treated as if it is transmitted.

The cross section of a spherical droplet is

$$a = \frac{\pi}{4} d^2, \tag{3.37}$$

and the number of droplets per volume unit is

$$n = \frac{1 - \alpha}{\frac{\pi}{6} d^3}, \tag{3.38}$$

where

a is the cross section of a droplet, m^2,

d the mean diameter of the droplet, m,

n the number of droplets per volume unit, m^{-3}, and

α the void fraction, dimensionless.

Combining (3.37) and (3.38) we obtain

$$\sigma = \varepsilon_l a n = \frac{3}{2} \frac{1 - \alpha}{d} \varepsilon_l. \tag{3.39}$$

The droplet concentration will not be the same everywhere in a horizontal cross section of the fuel element. When energy is absorbed in the droplets they will evaporate, and if the steam production is higher in one part of the fuel element than in another, steam will flow from this part to the other, and the droplets will follow the steam flow. The cross flow will stop when the production of steam is the same everywhere. The local concentration of droplets is now calculated on the basis of the following assumption:

In a horizontal cross section of the fuel element the absorption of thermal radiation is constant.

When radiation passing the surface is neglected, the intensity of thermal radiation just outside a surface is (cf. fig. 3.6)

$$I_i = W_i + H_i, \tag{3.40}$$

where

I_i is the intensity just outside surface i, W/m^2.

Combining equations 3.40 and 3.19 we obtain

$$I_i = \frac{(2 - \varepsilon_i)W_i - \varepsilon_i S_i}{1 - \varepsilon_i}. \tag{3.41}$$

The absorption per volume unit just outside surface i is from equation 3.35

$$q_i = \sigma_i I_i = \sigma_i \frac{(2 - \varepsilon_i)W_i - \varepsilon_i S_i}{1 - \varepsilon_i}, \tag{3.42}$$

where

q_i is the absorption just outside surface i, W/m^3, and

σ_i the absorption coefficient just outside surface i, m^{-1}.

The basic assumption is that q_i is constant over the cross section, and using (3.39) we obtain

$$(1 - \alpha_i) \frac{(2 - \varepsilon_i)W_i - \varepsilon_i S_i}{1 - \varepsilon_i} = K, \tag{3.43}$$

where

K is a constant, W/m^2, and

α_i the void just outside surface i, dimensionless.

To each surface one can associate a volume

$$V_i = \frac{1}{4} A_i D_e \,, \tag{3.44}$$

where

V_i is the volume associated to surface i, m^3, and

D_e the hydraulic diameter, m,

and let V_o be the total volume.

$$V_o = \sum_{i=1}^{i=N} V_i \,. \tag{3.45}$$

The sum of water in each volume must equal the total amount of water

$$\sum_{i=1}^{i=N} (1 - \alpha_i)V_i = (1 - \alpha_o)V_o \,, \tag{3.46}$$

where

α_o is the mean void, dimensionless.

Combination of equations 3.43 and 3.46 gives

$$K = \frac{(1 - \alpha_o)V_o}{\sum_{i=1}^{i=N} \frac{(1 - \varepsilon_i)V_i}{(2 - \varepsilon_i)W_i - \varepsilon_i S_i}} \,, \tag{3.47}$$

and substituting this in (3.43) we obtain

$$(1 - \alpha_i) = (1 - \alpha_o) \frac{\frac{(1 - \varepsilon_i)V_o}{(2 - \varepsilon_i)W_i - \varepsilon_i S_i}}{\sum_{i=1}^{i=N} \frac{(1 - \varepsilon_i)V_i}{(2 - \varepsilon_i)W_i - \varepsilon_i S_i}} \,. \tag{3.48}$$

Under the assumption that for a beam between surface i and surface j the mean concentration, $1 - \frac{1}{2}(\alpha_i + \alpha_j)$, can be used, $\tau_{i,j}$ can be determined

$$\tau_{i,j} = \exp\left\{ - \frac{3}{4} \varepsilon_v \frac{2 - \alpha_i - \alpha_j}{d} R_{i,j} \right\} \,, \tag{3.49}$$

where

$R_{i,j}$ is the beam length from surface i to surface j, m.

It is worth noting that (3.48) predicts a low droplet concentration where the intensity of thermal radiation is high, and a high droplet concentration where the intensity is low. This is in agreement with experimental results[15] for fuel elements.

3.4. Energy Balance for the Fuel

In the fuel rods energy is transferred by thermal conduction, and the energy balance is given by the Fourier equation

$$\rho c \frac{\partial T}{\partial t} = \nabla \cdot (k \nabla T) + Q \,, \tag{3.50}$$

where

ρ is the density, kg/m^3,

c the heat-capacity, J/kg ^oC,

T the temperature, ^oC,

t the time, sec.,

∇ the nabla operator, m^{-1},

k the thermal conductivity, W/m ^oC, and

Q the energy production, W/m^3.

In order to solve equation 3.50 it is convenient to express it in cylindrical coordinates and assume rotational symmetry.

$$\rho c \frac{\partial T}{\partial t} = \frac{1}{r} \frac{\partial}{\partial r} \left(rk \frac{\partial T}{\partial r} \right) + \frac{\partial}{\partial z} \left(k \frac{\partial T}{\partial z} \right) + Q \,, \tag{3.51}$$

where

r is the radius, m, and

z the axial position, m.

The integration of equation 3.51 is based on a finite difference method, and integrating (3.51) over a volume element we obtain

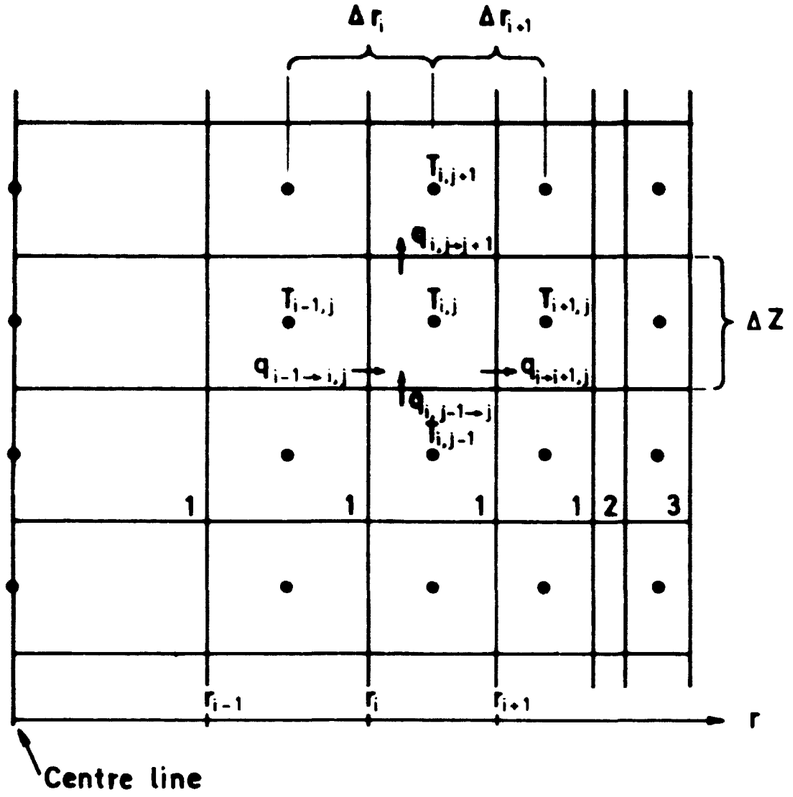

1. Fuel
2. Gas gap
3. Cladding

Fig. 3.9. Finite difference mesh for a fuel rod.

$$\Delta V_{i,j}(\rho c)_{i,j}\frac{\partial T_{i,j}}{\partial t} = q_{i-1\to i,j} - q_{i\to i+1,j} + q_{i,j-1\to j} - q_{i,j\to j+1} + Q_{i,j}\Delta V_{i,j}, \quad (3.52)$$

$$q_{i-1\to i,j} = 2\frac{k_{i-1,j}\,k_{i,j}}{k_{i-1,j}+k_{i,j}}\frac{T_{i-1,j}-T_{i,j}}{\Delta r_i}2\pi r_i\Delta z,$$

$$q_{i\to i+1,j} = 2\frac{k_{i,j}\,k_{i+1,j}}{k_{i,j}+k_{i+1,j}}\frac{T_{i,j}-T_{i+1,j}}{\Delta r_{i+1}}2\pi r_{i+1}\Delta z,$$

$$q_{i,j-1\to j} = 2\frac{k_{i,j-1}\,k_{i,j}}{k_{i,j-1}+k_{i,j}}\frac{T_{i,j-1}-T_{i,j}}{\Delta z}\pi(r_{i+1}^2 - r_i^2),$$

$$q_{i,j\to j+1} = 2\frac{k_{i,j}\,k_{i,j+1}}{k_{i,j}+k_{i,j+1}}\frac{T_{i,j}-T_{i,j+1}}{\Delta z}\pi(r_{i+1}^2 - r_i^2). \quad (3.53)$$

At the surface $q_{i\to i+1,j}$ must be replaced by the heat transfer to the fluid as calculated in subsections 3.3.1 and 3.3.2. The material parameters in equations 3.52 and 3.53 and the heat transfer coefficient in the gas gap may be temperature dependent.

For the shroud a similar technique is used.

The integration of equation 3.52, which is in a conserving form, in time is performed using an explicit integration technique.

3.5. Mass, Momentum, and Energy Balance for the Two-Phase Flow

The continuity, momentum, and energy equation together with the equation of state are solved for the steam and water phase. Thermal equilibrium is not assumed, and the interchange of mass, momentum, and energy between the phases is considered.

3.5.1. Film Flow

The spray water injected in the upper plenum will generate a film flow on the fuel rods and on both sides of the shroud. At the quench front the film will leave the surface on account of sputtering.

Between the top of the fuel element and the quench front the film flow is evaluated on the following assumptions:

1. The film flow is assumed to be quasi-stationary, i.e. $\frac{\partial v}{\partial t} = 0$. This is justified by the fact that the time constant for perturbations is smaller than approximately 0.1 sec.
2. The friction between the film and the steam flow is negligible compared with the wall friction.

For a given film thickness the film flow is determined by [16]

$$G_f = - \frac{\rho_l^2 g}{3\mu_l} s_f^3 , \qquad (3.54)$$

where

G_f is the film flow, kg/m sec.,

ρ_l the density of water, kg/m^3,

g the acceleration of gravity, m/sec.^{2},

μ_l the viscosity of water, kg/m sec., and

s_f the film thickness, m.

The continuity and energy equations are

$$\frac{\partial}{\partial t}(s_f \rho_l) = - \frac{\partial}{\partial z}(G_f) - \dot{m}_f \qquad (3.55)$$

$$\frac{\partial}{\partial t}(s_f \rho_l h_f) = - \frac{\partial}{\partial z}(G_f h_f) + q_{wf} - q_{fg} - \dot{m}_f h_{sg} , \qquad (3.56)$$

where

$\dot{m}_f$ is the evaporation/condensation rate (see subsection 3.3.4), kg/m^2 sec.,

h_f the specific enthalpy of the film, J/kg,

q_{wf} the heat flux from the wall to the film, W/m^2,

q_{fg} the heat flux from the film to the steam (cf. eq. 3.5), W/m^2, and

h_{sg} the specific enthalpy of saturated steam, J/kg.

The continuity and energy equations are integrated using an explicit backward method.

3.5.2. Drop Flow

Droplets will be produced directly from the spray system and secondarily from sputtering in the quench front. Depending on the size of the

droplets and the steam flow a droplet will either fall down through the fuel element or as entrained liquid follow the steam flow.

3.5.2.1. The Spray System and the Droplet Production

A liquid jet formed at the spray nozzles will break down to droplets owing to the Rayleigh instability [17]. If the Weber number of the droplets is too high, they will break up in a number of smaller droplets.

A small perturbation on a liquid jet will grow exponentially, and if we neglect the viscosity, the growth rate will be determined by

$$\omega^2 = \frac{\sigma}{2\rho_l r_j^3}(\lambda r_j)^2 \left\{1 - (\lambda r_j)^2 + \lambda r_j \frac{We_j}{2}\right\}, \qquad (3.57)$$

$$We_j = \frac{2 r_j \rho_g (u_j - u_g)^2}{\sigma}, \qquad (3.58)$$

where

ω^{-1} is the time constant, sec.,

σ the surface tension, N/m,

ρ_l the density of water, kg/m^3,

r_j the radius of the jet, m,

λ the wave number of the perturbation, m^{-1},

We_j the Weber number of the jet, dimensionless,

ρ_g the density of steam, kg/m^3,

u_j the velocity of the jet, m/sec., and

u_g the velocity of the steam, m/sec.

From equation 3.57 it is easily seen that the maximum growth rate occurs for

$$\lambda r_j = \frac{3}{16} We_j + \sqrt{\left(\frac{3}{16} We_j\right)^2 + \frac{1}{2}}. \qquad (3.59)$$

Comparison with experiments [16, 24] shows that a liquid jet will break up in accordance with equation 3.59, and from (3.59) the diameter of the produced droplets is obtained:

$$d_d = 2r_j \left\{ \frac{3\pi}{\frac{3}{8} We_j + \sqrt{(\frac{3}{8} We_j)^2 + 2}} \right\}^{\frac{1}{3}}, \qquad (3.60)$$

where

d_d is the droplet diameter, m.

From equations 3.57 and 3.59 the length of the jet can be determined

$$L_j = r_j \ln (\frac{r_j}{\Delta r}) \sqrt{\frac{\rho_1}{\rho_g}} \frac{\sqrt{We_j}}{\left\{\frac{3}{16} We_j + \sqrt{(\frac{3}{16} We_j)^2 + \frac{1}{2}}\right\}\left\{\frac{1}{2} + \frac{3}{128} We_j^2 + \frac{We_j}{8}\sqrt{\frac{3}{16} We_j)^2 + \frac{1}{2}}\right\}^{\frac{1}{2}}} \qquad (3.61)$$

where

L_j is the length of the jet, m, and

Δr the initial perturbation, m.

From experiments [23] it has been found that

$$\ln (\frac{r_j}{\Delta r}) \approx 15.7. \qquad (3.62)$$

The derivation of equation 3.61 was based on the assumption of negligible viscosity in the jet and laminar flow in the steam. The viscosity will tend to increase the length, but on the other hand violent turbulence in the steam will decrease it.

The produced droplets will have aWeber number given by

$$We_d = \frac{d_d \rho_g (u_d - u_g)^2}{\sigma} \qquad (3.63)$$

$$u_d = u_j,$$

where

We_d is the Weber number of the droplets, dimensionless, and

u_d the velocity of the droplets, m/sec.

Owing to the motion of the droplet the pressure distribution around it will be non-uniform, and the droplet will be deformed.

The deformation of the droplet is determined by

$$P_o + P_s = \text{const.}, \tag{3.64}$$

where

P_o is the pressure outside the droplet, N/m^2, and

P_s the pressure arising from the surface tension, N/m^2.

From equation 3.64 and on the assumption that the droplet has the shape of an ellipsoid, the deformation is obtained

$$a^{\frac{1}{2}} + a^{-\frac{5}{2}} - 2a^2 = \dot{C}_D \, We_d , \tag{3.65}$$

$$a = \frac{d_u}{d_d} ,$$

$$\dot{C}_D = \min (0.5, C_D) ,$$

where

d_u is the thickness of the droplet in the direction of motion, m, and

C_D the drag coefficient, dimensionless.

$$C_D = \begin{cases} \dfrac{24}{Re_d} & \text{for } Re_d \leq 0.71 \\ 0.4 + 25.4\, Re_d^{-0.8} & \text{for } Re_d > 0.71 \end{cases} \tag{3.66}$$

$$Re_d = \frac{d_d \rho_g | u_d - u_g |}{\mu_g} , \tag{3.67}$$

where

Re_d is the Reynolds number of the droplet, dimensionless, and

μ_g the viscosity of steam, kg/m sec.

Maintaining the surface energy, the deformed droplet will break up into n spherical droplets

$$n = \left\{ \frac{1}{2a} + \sqrt{a} \, \frac{\ln \left(a^{-\frac{3}{2}} + \sqrt{a^{-3} - 1} \right)}{2\sqrt{a^{-3} - 1}} \right\}^3 , \tag{3.68}$$

and the diameter of the daughter droplets is

$$\dot{d}_d = d_d\, n^{-\frac{1}{3}} . \qquad (3.69)$$

A droplet can break up into at least two smaller droplets, and if this is the case a critical Weber number, We_c, can be determined from equations 3.65 and 3.68:

$$We_c = 13.1 \qquad \text{for } C_D = 0.5.$$

Which is in excellent agreement with experiments [16].

The movement and deformation of the droplet are determined by the following set of equations:

Continuity

$$\frac{dm_d}{dt} = -\dot{m}_d \qquad (3.70)$$

Momentum

$$\frac{d}{dt}(m_d u_d) = -\frac{1}{2}\rho_g (u_d - u_g)\,|u_d - u_g|\,\frac{\pi d_d^2}{4a}\,C_D - \dot{m}_d \dot{u}_d - m_d g \qquad (3.71)$$

$$\dot{u}_d = \begin{cases} u_d & \text{for } \dot{m}_d > 0 \\ u_g & \text{for } \dot{m}_d \leq 0 \end{cases} \qquad (3.72)$$

Energy

$$\frac{d}{dt}(m_d h_d) = -q_{dg} - \dot{m}_d h_{sg} \qquad (3.73)$$

Deformation

$$\frac{d^2 a}{dt^2} = -9\left(\frac{u_d - u_g}{d_d}\right)^2 \frac{\rho_g}{\rho_l}\left\{\dot{C}_D + \frac{1}{We_d}(2a^2 - \sqrt{a} - a^{-\frac{5}{2}})\right\}\sqrt{a} \qquad (3.74)$$

where

m_d is the mass of the droplet, kg,

$\dot{m}_d$ the evaporation/condensation from the droplet, kg/sec.,

h_d the specific enthalpy of the droplet, J/kg,

h_{sg} the specific enthalpy of saturated steam, J/kg,

g the acceleration of gravity, m/sec.^{2}, and

q_{dg} the heat transfer from the droplet surface to the steam, W/m^2.

The heat transfer q_{dg} to the steam and the evaporation term are determined as shown in subsection 3.3.4.

An integration of the equations 3.70 - 3.74 together with the relations (3.65), (3.68), and (3.69) determines the entire transient of a droplet. The integration is performed using a second-order integration technique [18].

Let d_{df} be the final dimension of the droplets produced from the spray system. In reality d_{df} will not be the only dimension as a certain spectrum of droplet sizes will exist [16].

$$p(d) = \frac{4}{3d_o^3}\, d^2\, e^{-\frac{2}{d_o} d}\,, \qquad (3.75)$$

$$d_o = \frac{1}{2} d_{df}\,,$$

where

d_{df} is the final diameter of the droplets, m, and

$p(d)$ the probability density function.

The minimum size of droplets able to fall down against an upward flow of steam is determined by

$$\frac{\pi}{6} d_c^3 \rho_l g = \frac{1}{2}\rho_g u_g^2 \frac{\pi}{4} d_c^2 C_D\,, \qquad (3.76)$$

where

d_c is the minimum droplet size, m.

The fraction [16] of droplets carried away with the steam flow is then

$$\eta = \frac{\int_0^{d_c} d^3 \upsilon(d)dd}{\int_0^{\infty} d^3 p(d)dd} \quad . \tag{3.77}$$

The mean size of droplets following the steam flow and of droplets falling against the steam flow is then obtained

$$d_d^+ = \frac{\int_0^{d_c} d^3 p(d)dd}{\int_0^{d_c} d^2 p(d)dd} \quad , \tag{3.78}$$

$$d_d^- = \frac{\int_{d_c}^{\infty} d^3 p(d)dd}{\int_{d_c}^{\infty} d^2 p(d)dd} \quad , \tag{3.79}$$

where

d_d^+ is the dimension of the droplets following the steam flow, m, and

d_d^- the dimension of the droplets falling against the steam flow, m.

Droplets are also produced in the quench front owing to sputtering. The typical size of the droplets is 1 - 2 mm [19].

3.5.2.2. Drop Flow in the Primary System

The drop flow in the primary system is calculated taking into account the conservation of mass, momentum, and energy and the exchange of mass, momentum, and energy with the steam phase, together with the equation of state.

Continuity

$$\frac{\partial}{\partial t}(m_d) = -\frac{\partial}{\partial z}(u_d\, m_d) - \dot{m}_d + G_d \tag{3.80}$$

Momentum

$$\frac{\partial}{\partial t}(m_d u_d) = -\frac{\partial}{\partial z}(m_d u_d^2) - \dot{b} - (m_d - \alpha_i \rho_g)g - \dot{m}_d \grave{u}_d + B_d \tag{3.81}$$

Energy

$$\frac{\partial}{\partial t}(m_d\, h_d) = -\frac{\partial}{\partial z}(u_d m_d h_d) - q_{dg} - \dot{m}_d h_{sg} + H_d \tag{3.82}$$

$$\grave{u}_d = \begin{cases} u_d & \text{for } \dot{m}_d > 0 \\ u_g & \text{for } \dot{m}_g \leq 0 \end{cases} \tag{3.83}$$

where

m_d is the mass per volume, kg/m^3,

u_d the velocity of droplets, m/sec.,

u_g the velocity of steam, m/sec.,

$\dot{m}_d$ the evaporation/condensation, kg/sec. m^3,

G_d a source term, e.g. sputtering, kg/sec. m^3,

$\dot{b}$ the interchange of momentum with the steam, kg/m^2 $sec.^2$,

α_i the volume fraction of droplets, dimensionless,

ρ_g the density of steam, kg/m^3,

g the acceleration of gravity, $m/sec.^2$,

B_d a source, kg/m^2 $sec.^2$,

h_d the specific enthalpy of the droplets, J/kg,

q_{dg} the heat transfer from the droplets to the steam, W/m^3,

H_d a source, W/m^3, and

h_{sg} the specific enthalpy of saturated steam, J/kg.

The dimension of the droplets may change, and neglecting fusion and split-up the number of the droplets has to be maintained.

$$\frac{\partial}{\partial t}(n_d) = -\frac{\partial}{\partial z}(n_d u_d) + N_d \,, \tag{3.84}$$

where

u_d is the number of droplets per volume, m^{-3}, and

N_d a source, e.g. the spray system, m^{-3}.

The source terms in equations 3.80 - 3.84 are either the spray system or the sputtering of a film in a quench front, and in either case the dimension, velocity, and temperature of the produced droplets are known.

The evaporation from the droplets and the heat transfer to the steam are determined as described in subsection 3.3.4. The interchange of momentum with the steam is determined by

$$\dot{b} = n_d \tfrac{1}{2}\rho_g |u_d - u_g| (u_d - u_g) \tfrac{\pi}{4} d_d^2 C_D \,, \tag{3.85}$$

$$d_d = \left(\frac{6 m_d}{\rho_l \pi n_d}\right)^{\frac{1}{3}} \,, \tag{3.86}$$

where

d_d is the diameter of the droplets, m,

C_D the drag coefficient (cf. eq. 3.66), and

ρ_l the density of water kg/m^3.

The volume fraction of droplets is given by

$$\alpha_i = 1 - \alpha = \frac{m_d}{\rho_l} \,, \tag{3.87}$$

where

α is the void, dimensionless.

The entire set of equations describing the drop flow is integrated using an explicit backward integration technique.

3.5.3. Steam Flow

The steam flow in the primary system is based on a solution of the equation for conservation of mass, momentum, and energy and the interchange of mass, momentum, and energy between the phases, together with the equation of state.

Continuity

$$\frac{\partial \rho_g}{\partial t} = -\frac{\partial}{\partial z}(\rho_g u_g) + \dot{m}_g + G_g \tag{3.88}$$

Momentum

$$\frac{\partial}{\partial t}(\rho_g u_g) = -\frac{\partial}{\partial z}(\rho_g u_g^2) - \frac{\partial P}{\partial z} - \rho_g g - \frac{\partial F_g}{\partial z} + \dot{b} + \dot{m}_g u_g' + B_g \tag{3.89}$$

$$u_g' = \begin{cases} u_l \text{ x)} & \text{for } \dot{m}_g > 0 \\ u_g & \text{for } \dot{m}_g < 0 \end{cases} \tag{3.90}$$

Energy

$$\frac{\partial}{\partial t}(\rho_g(h_g - \frac{P}{\rho_g} + \tfrac{1}{2}u_g^2 + zg)) = -\frac{\partial}{\partial z}(\rho_g u_g(h_g + \tfrac{1}{2}u_g^2 + zg)) + q_{lg} + \dot{m}_g(h_{sg} + \tfrac{1}{2}u_g'^2 + zg) + H_g \tag{3.91}$$

Equation of state

$$T_g = T_g(h_g, P) \tag{3.92}$$

where

ρ_g is the density of steam, kg/m^3,

u_g the velocity of steam, m/sec.,

$\dot{m}_g$ evaporation/condensation, kg/m^3 sec.,

G_g a source, e.g. pool boiling in lower plenum, kg/m^3 sec.,

x) The liquid may be films or droplets

P the pressure, N/m^2,

g the acceleration of gravity, $m/sec.^2$,

$\frac{\partial F_g}{\partial z}$ the wall friction, $kg/m\ sec.^2$,

$\dot{b}$ momentum interchange with the liquid, $kg/m^2\ sec.^2$,

u_l the velocity of water, m/sec.,

B_g a source, $kg/m^2\ sec.^2$,

h_g the specific enthalpy of steam, J/kg,

q_{lg} the heat transfer between liquid and steam (cf. subsection 3.3.4), W/m^3

h_{sg} the specific enthalpy of saturated steam, J/kg, and

H_g a source, e.g. heat transfer from the fuel, W/m^3.

If we neglect the terms representing the interchange between the water and steam phase, it can be shown that equations 3.88 to 3.92 have the eigenvalues [20, 30]

$$\lambda = \begin{cases} u_g \\ u_g + c \\ u_g - c \end{cases} \qquad (3.93)$$

$$c = \frac{\frac{P}{\rho_g^2} \cdot \frac{\partial e_g}{\partial \rho_g}}{\frac{\partial e_g}{\partial P}} , \qquad (3.94)$$

where

λ is the eigenvalues, m/sec.,

c the velocity of sound in steam, m/sec., and

e_g the internal energy of steam, J/kg.

c will normally be in the range of several hundred m/sec., whereas u_g will be a few m/sec. For core heat-up and emergency core cooling transients phenomena related to the velocity of sound are unimportant and of no interest, and without introducing any significant error we can assume that c is infinite, i.e. the medium is considered incompressible. It can easily be shown that this assumption leads to [30]

$$\frac{\partial u_g}{\partial t} = 0 \tag{3.95}$$

$$\frac{\partial P}{\partial t} = 0 \, . \tag{3.96}$$

Using (3.95) and (3.96) in the momentum and energy equation we obtain

$$u_g \frac{\partial \rho_g}{\partial t} = - \frac{\partial}{\partial z} (\rho_g u_g^2) - \frac{\partial P}{\partial z} - \rho_g g - \frac{\partial F}{\partial z} + \dot{b} + \dot{m}_g \dot{u}_g + B_g \tag{3.97}$$

$$\frac{\partial h_g}{\partial t} \left(\rho_g + \frac{h_g + \frac{1}{2} u_g^2 + zg}{\left. \frac{\partial h_g}{\partial \rho_g} \right|_P} \right) = - \frac{\partial}{\partial z} (\rho_g u_g (h_g + \tfrac{1}{2} u_g^2 + zg)) + q_{lg}$$

$$+ \dot{m}_g (h_{sg} + \tfrac{1}{2} u_g^2 + zg) + H_g \tag{3.98}$$

$$\frac{\partial h_g}{\partial t} = \left. \frac{\partial h_g}{\partial \rho_g} \right|_P \frac{\partial \rho_g}{\partial t} \, . \tag{3.99}$$

In equation 3.98 the term $\frac{1}{2} u_g^2 + zg$ is normally neglected.

The assumption of infinite velocity of sound has the advantage that the computation time may be decreased by a factor of 10 to 100 without introducing errors.

The interchange of mass, momentum, and energy between the phases is calculated as described in subsections 3.5.1 and 3.5.2. The wall friction is obtained through

$$\Delta z \frac{\partial F_g}{\partial z} = \frac{1}{2} \rho_g u_g | u_g | (4 \Delta z \frac{C_F}{D_e} + V_h) \tag{3.100}$$

$$C_F = \begin{cases} \dfrac{16}{Re_g} & \text{for laminar flow} \\ 0.0792\ Re_g^{-0.25} & \text{for turbulent flow} \end{cases} \qquad (3.101)$$

$$Re_g = \frac{\rho_g D_e |u_g|}{\mu_g}, \qquad (3.102)$$

where

C_F is the friction factor, dimensionless,

D_e the hydraulic diameter, m,

V_h velocity heads, representing spacers, orifices, etc., dimensionless,

Re_g Reynolds' number for the steam, dimensionless, and

μ_g the viscosity of steam, kg/m sec.

In the model equations 3.88, 3.97, and 3.98 are integrated using an explicit backward method.

3.6. Thermodynamic Properties

The properties of steam and water are evaluated using polynomial approximations [21]. The polynomials, many of which are in two variables, are developed to fit the tables with an error of less than 5 o/oo.

The thermodynamic properties of fuel, cladding, and the structural materials are in the same way calculated by means of polynomials.

3.7. Computing Times

The computation time for the calculation of a core heat-up and emergency core cooling transient is naturally dependent on the size and complexity of the problem, but typically for problems as those in chapters 4 and 5 the ratio between the computer time and real time for the B 6700-computer at Risø is about 10.

4. BWR-FLECHT CALCULATIONS

In order to examine the applicability of the computer code RHC for calculation of core heat-up and emergency core cooling transients, it was compared with experiments. For this purpose the BWR-FLECHT SS4N[10,11] test series was chosen. This test series consists of a number of core heat-up and emergency core cooling transients with an electrically heated fuel element for pressures between 1 and 21 bar.

Naturally it would have been better to compare it with a transient for a nuclear power reactor, but none such exists. For fuel elements simulated by electrically heated rods a variety of experiments exist, but generally they have been performed at atmospheric pressure, which is unrealistic, and the documentation is very poor. Taking these objections into account, the BWR-FLECHT SS4N test series was chosen to be the best. However, also for these experiments the documentation is insufficient, and a number of assumptions had to be made in order to perform the comparison. Furthermore nothing is known about the uncertainty in the measurements. Consequently the results of the comparison must be considered with caution.

Generally the comparisons show that the computer code RHC is able to predict the maximum temperature of a core heat-up and emergency core cooling transient to within 60°C.

4.1. Description of BWR-FLECHT Test Facility

The BWR-FLECHT test facility[10] consists of a full scale 7 x 7 array of electrically heated fuel rods mounted with 8 BWR-spacers (cf. fig. 4.1). The rods are indirectly heated, and the cladding material is stainless steel. An outer channel was constructed around the shroud in order to allow film flow on both sides of the shroud. The spray water is injected above the bundle, and the produced steam and excess spray water are extracted at the bottom of the bundle. In table 4.1 are shown the main data of the test facility, and in figs. 4.2 and 4.3 the axial and the local power peaking of the rods. The local power peaking for the four-group model used in RHC calculations (cf. fig. 4.3) is shown in table 4.2. The energy production versus the time after transient initiation is shown in fig. 4.4.

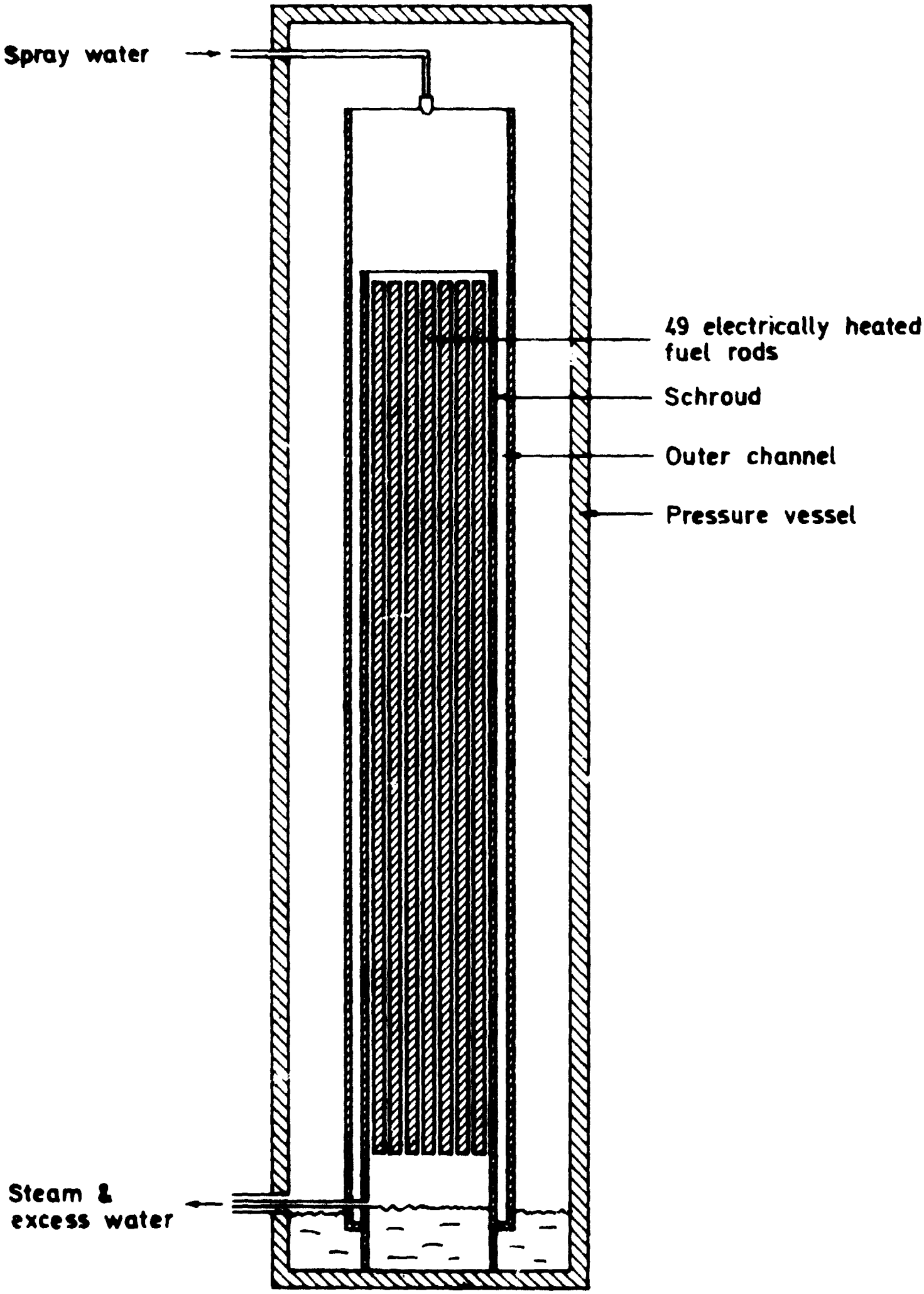

Fig. 4.1. Schematic diagram of BWR - FLECHT test facility.

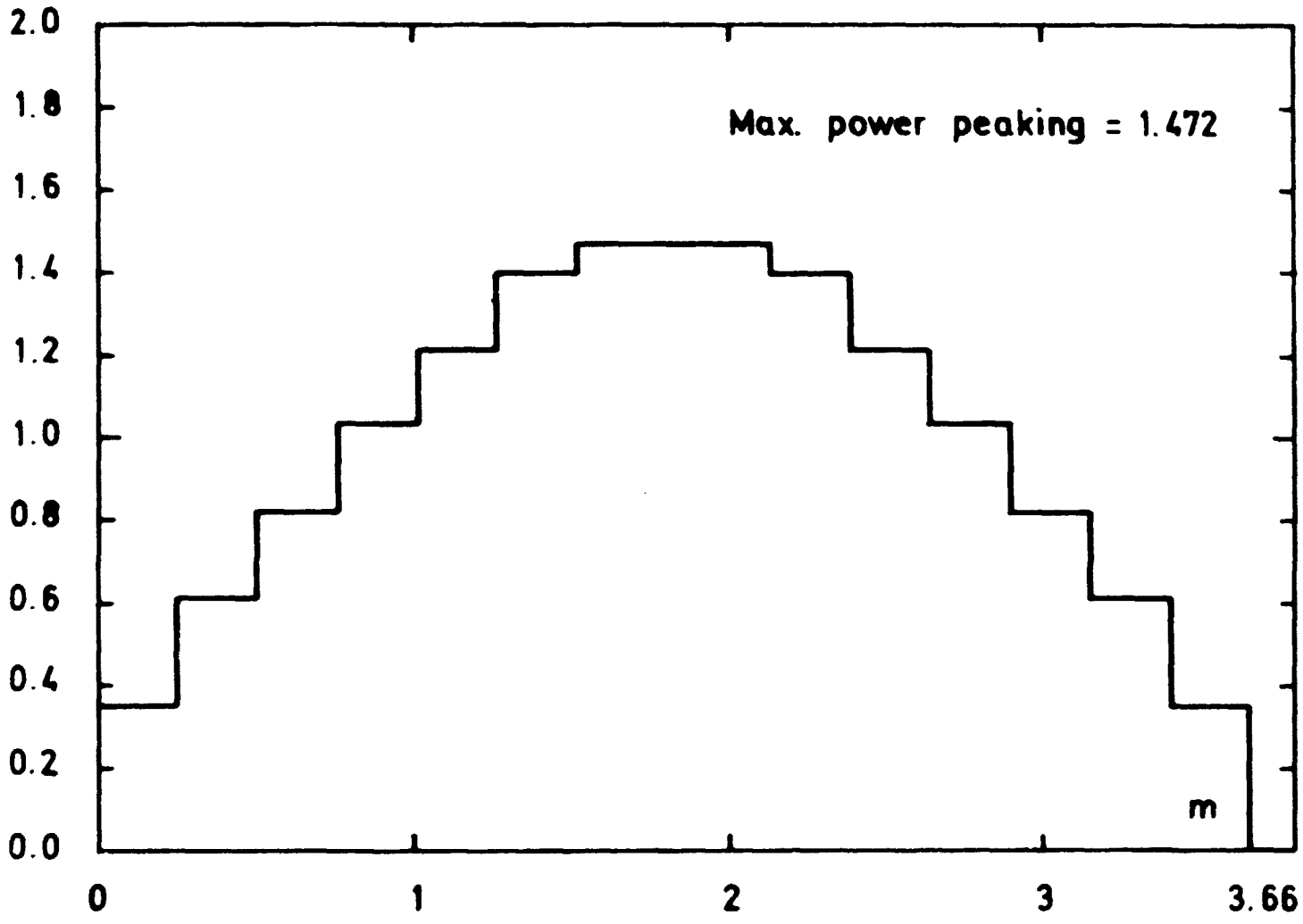

Fig. 4.2. Axial profile of BWR - FLECHT element.

1 1.06 4	2 1.12 3	3 0.98 3	4 1.15 3	5 1.13 3	6 1.09 3	7 0.91 4
8 1.15 3	9 1.10 2	10 0.93 2	11 1.07 2	12 0.99 2	13 1.01 2	14 0.95 3
15 0.97 3	16 0.92 2	17 0.98 1	18 0.92 1	19 0.93 1	20 0.96 2	21 1.01 3
22 1.15 3	23 1.07 2	24 0.92 1	25 0.91 1	26 0.93 1	27 0.91 2	28 1.02 3
29 1.18 3	30 1.00 2	31 0.91 1	32 0.88 1	33 0.86 1	34 0.91 2	35 1.03 3
36 1.10 3	37 1.03 2	38 0.96 2	39 0.91 2	40 0.91 2	41 0.96 2	42 1.17 3
43 0.92 4	44 0.97 3	45 1.03 3	46 1.03 3	47 0.97 3	48 1.17 3	49 1.12 4

Fig. 4.3. Rod numbers, lokal power peaking, and rod groups.

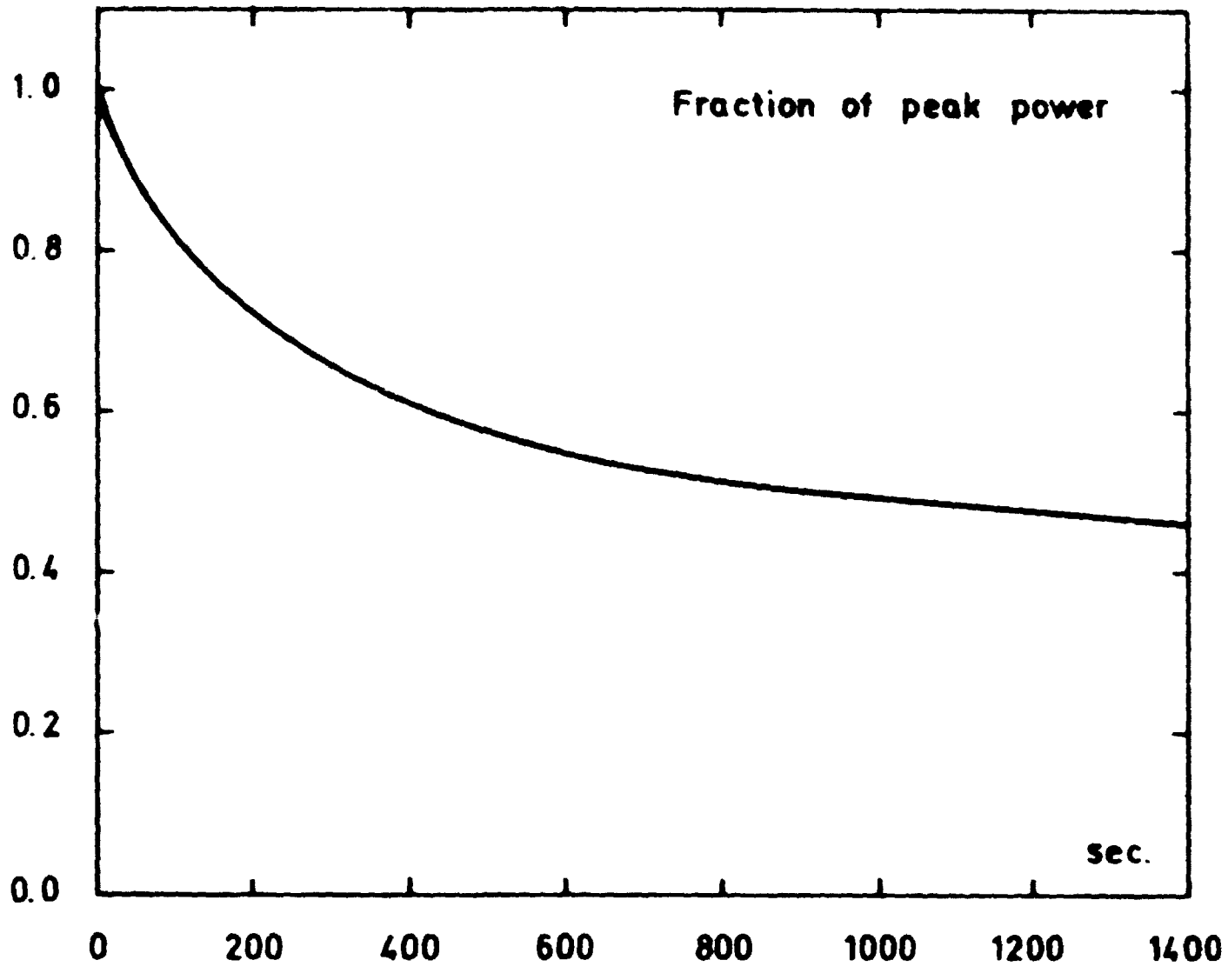

Fig. 4.4. Fraction of peak power.

Table 4.1

BWR-FLECHT data

Fuel rod length, m	3.66	
Fuel rod outside diameter, m	$1.448 \cdot 10^{-2}$	
Cladding thickness, m	$2.54 \cdot 10^{-3}$	
Fuel rod pitch, m	$1.875 \cdot 10^{-2}$	
Inside dimension of channel, m	0.134	
Channel wall thickness, m	$2.032 \cdot 10^{-3}$	
Flow area, m^2	$9.906 \cdot 10^{-3}$	
Peak power, W	$2.5 \cdot 10^{5}$	
Spray water flow rate, kg/sec.	0.148	x)
Spray water subcooling, ^{o}C	35.0	+)
Stainless-steel surface emissivity	0.5	
Emissivity of water	0.96	

x) corresponds to 2.45 gpm.
+) assumed value.

Table 4.2

Local power peaking in 4 group model

Group	No. of rods	Local power peaking
1	9	0.9103
2	16	0.9722
3	20	1.0632
4	4	0.9972

4.2. Comparison of Experimental Data and RHC Calculations

Calculations of core heat-up and emergency core cooling transients were performed with the RHC computer code for four of the spray cooling experiments at the BWR-FLECHT SS4N test facility. The four experiments chosen for comparison were performed at 2.07, 4.14, 6.205, and 13.79 bar, and the data from these experiments are compared with the calculations. For run 5x, at a pressure of 4.14 bar, are given some more detailed results of the calculations although experimental data for comparisons are not available. This is done merely as a demonstration of the capabilities of the model.

In table 4.3 are shown the maximum temperatures for the BWR-FLECHT fuel element, and in table 4.4 and fig. 4.17 the maximum temperatures for the different rod groups for run 5x.

Table 4.3

Comparison with BWR-FLECHT experiments

Maximum temperature for group 1 rods

Run	Pressure bar	Tmax. ex.[x] °C	Tmax. RHC °C
4	2.07	1084	1016
5x	4.14	1090	1033
6	6.205	1067	1033
8(2)	13.79	950	1018

[x] average for group 1 rods.

Table 4.4

Comparisons of max. temperatures, run 5x

Rod group	Measurements[x] °C	RHC calculation °C
1	1090	1033
2	998	992
3	831	913
4	762	849

[x] average for the group.

From table 4.3 it is seen that the model is able to predict the maximum temperature with an error of approximately 60°C, and it is seen in agreement with subsection 3.3.1 that the model tends to overpredict the maximum temperature at heigh pressures. From table 4.4 and fig. 4.17 it is seen that the model underpredicts the temperatures for the central rods, and overpredicts the temperatures for the rods near the shroud, i.e. the calculated horizontal temperature profile is more flat than the profile actually observed. This is due to an inaccuracy in one of the main assumptions in the model for radiation heat transfer (cf. subsection 3.3.5), namely that all surfaces emit radiation uniformly, which is obviously not valid for a rod near the shroud. As a result of this assumption the radiation heat transfer between the individual rods is overpredicted, while the error in the net radiation heat transfer between all the rods and the shroud is minor. Consequently the model will predict a horizontal temperature distribution among the rods which is too flat. In order to avoid this calamity a transport correction of the radiation heat transfer may be suggested.

In figs. 4.5 - 4.8 are shown the temperature transients at the bundle midplane for the four cases considered. The dotted line is the measured temperature at the midplane for rod no. 17 (cf. fig. 4.3), and an excellent agreement is observed. The somewhat poorer agreement between the measured and calculated transient for run 8(2) is mainly due to differences in the wetting times (cf. tables 4.5 and 4.6). This arises chiefly from the lack of knowledge about distribution of water from spray nozzles.

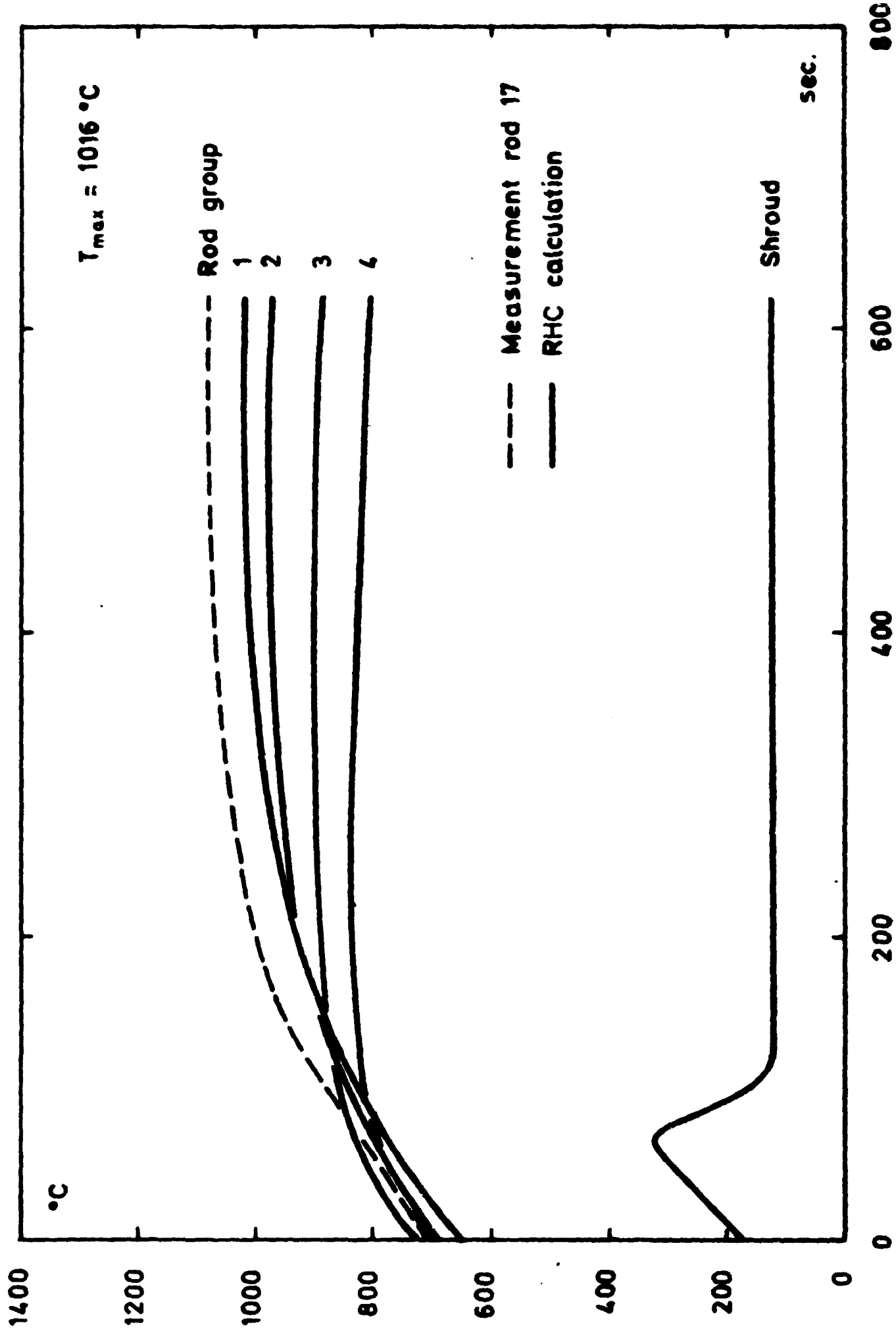

Fig. 4.5. BWR - FLECHT. run 4. Temperatures at fuel element midplane.

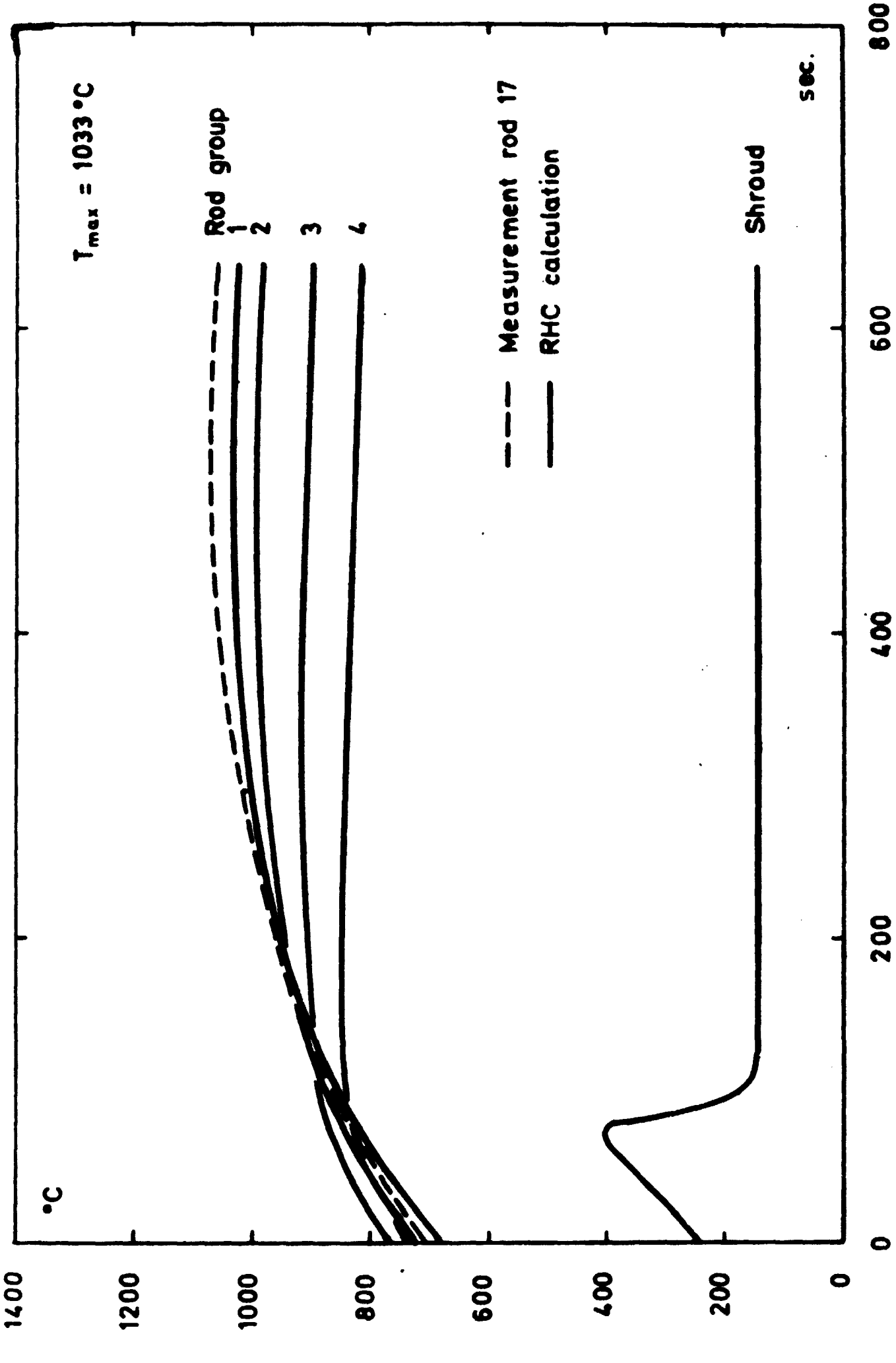

Fig. 4.6. BWR - FLECHT. run 5x. Temperatures at fuel element midplane.

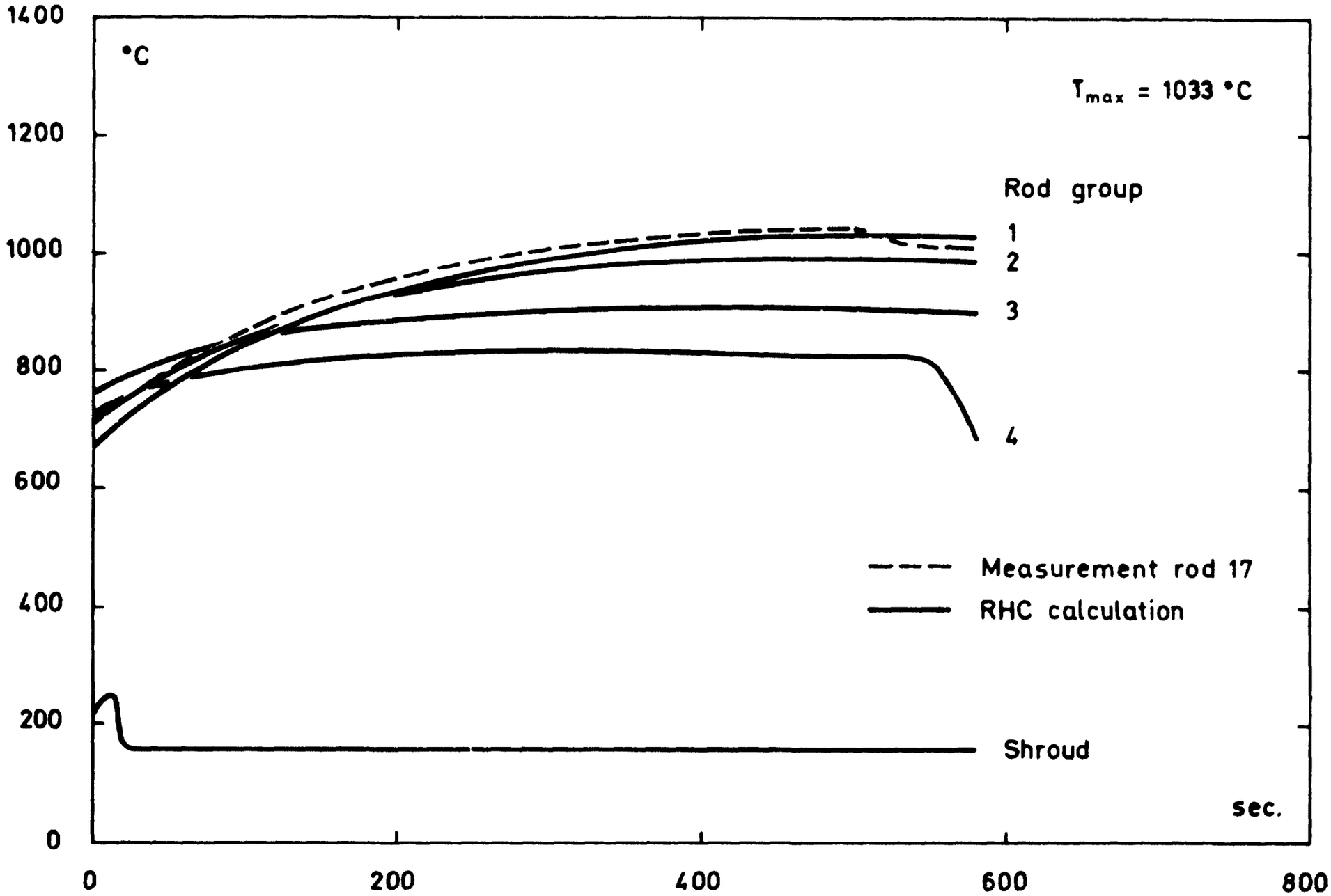

Fig. 4.7. BWR - FLECHT run 6. Temperatures at fuel element midplane.

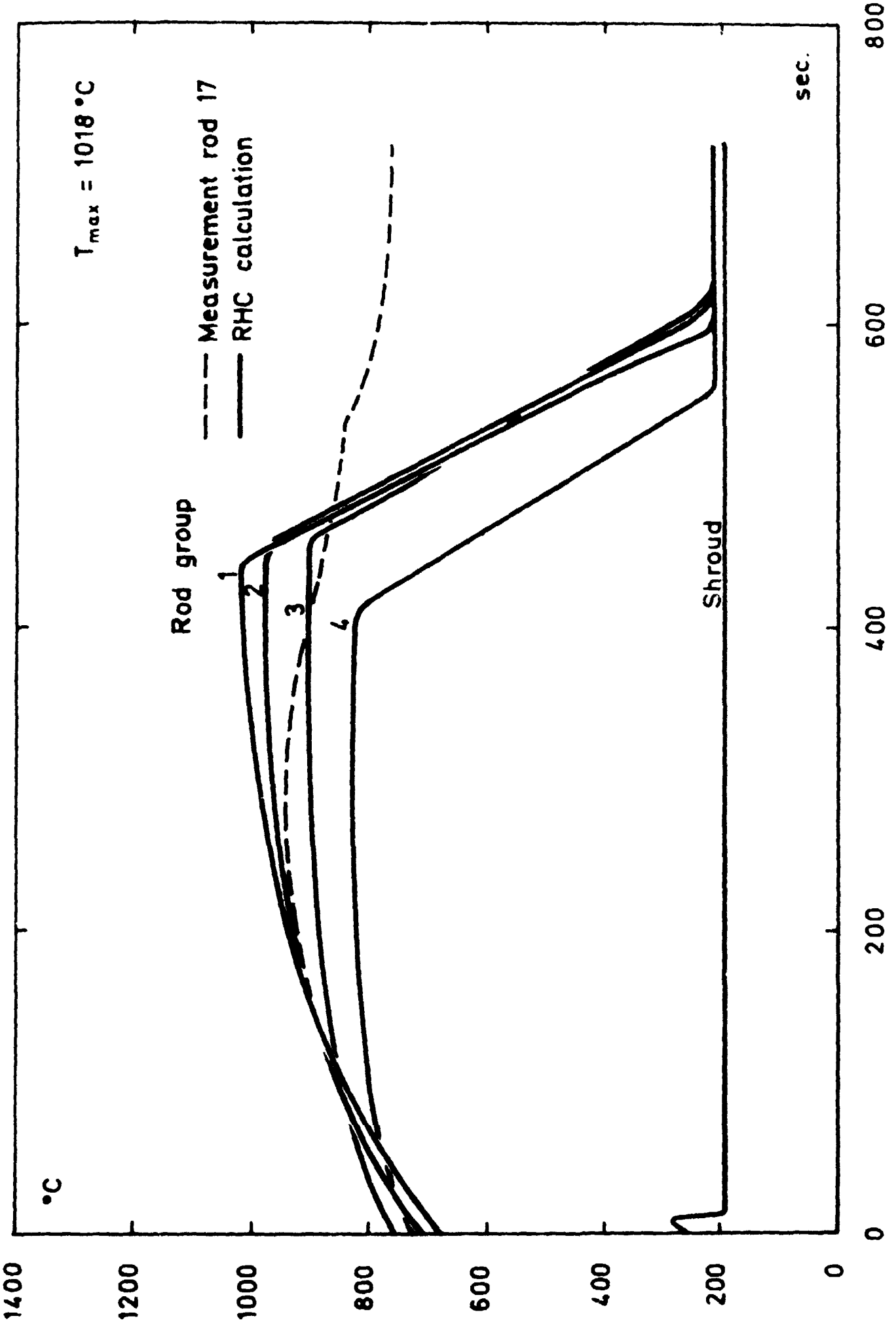

Fig. 4.8. BWR - FLECHT run 8(2). Temperatures at fuel element midplane.

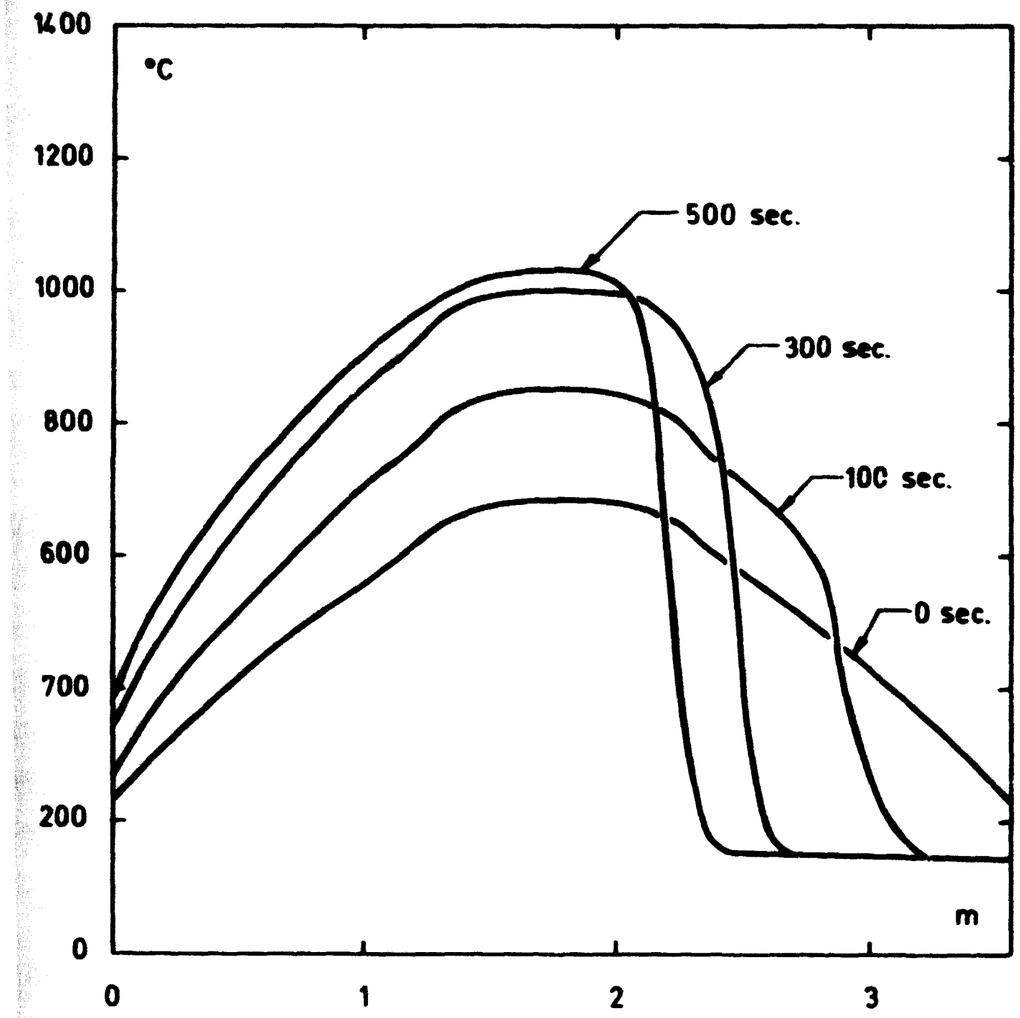

Fig. 4.9. BWR - FLECHT run 5x. Temperature profiles for group 1.

The axial temperature profiles for run 5x at 0, 100, 300, and 500 seconds after transient initiation for the individual rod groups and the shroud are shown in figs. 4.9 - 4.13. The sudden temperature drop which is seen for both the rods and the shroud is due to the advancing film front.

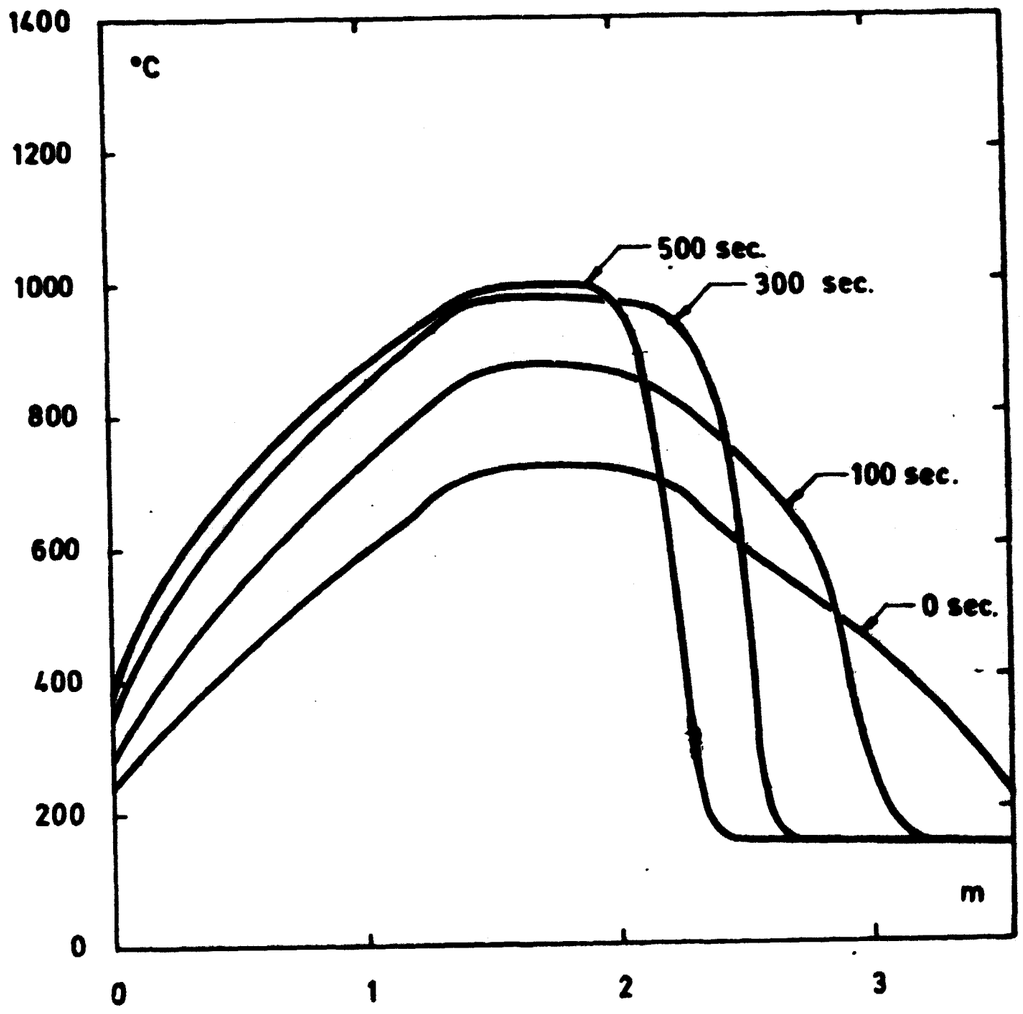

Fig. 4.10. BWR - FLECHT run 5x. Temperature profiles for group 2.

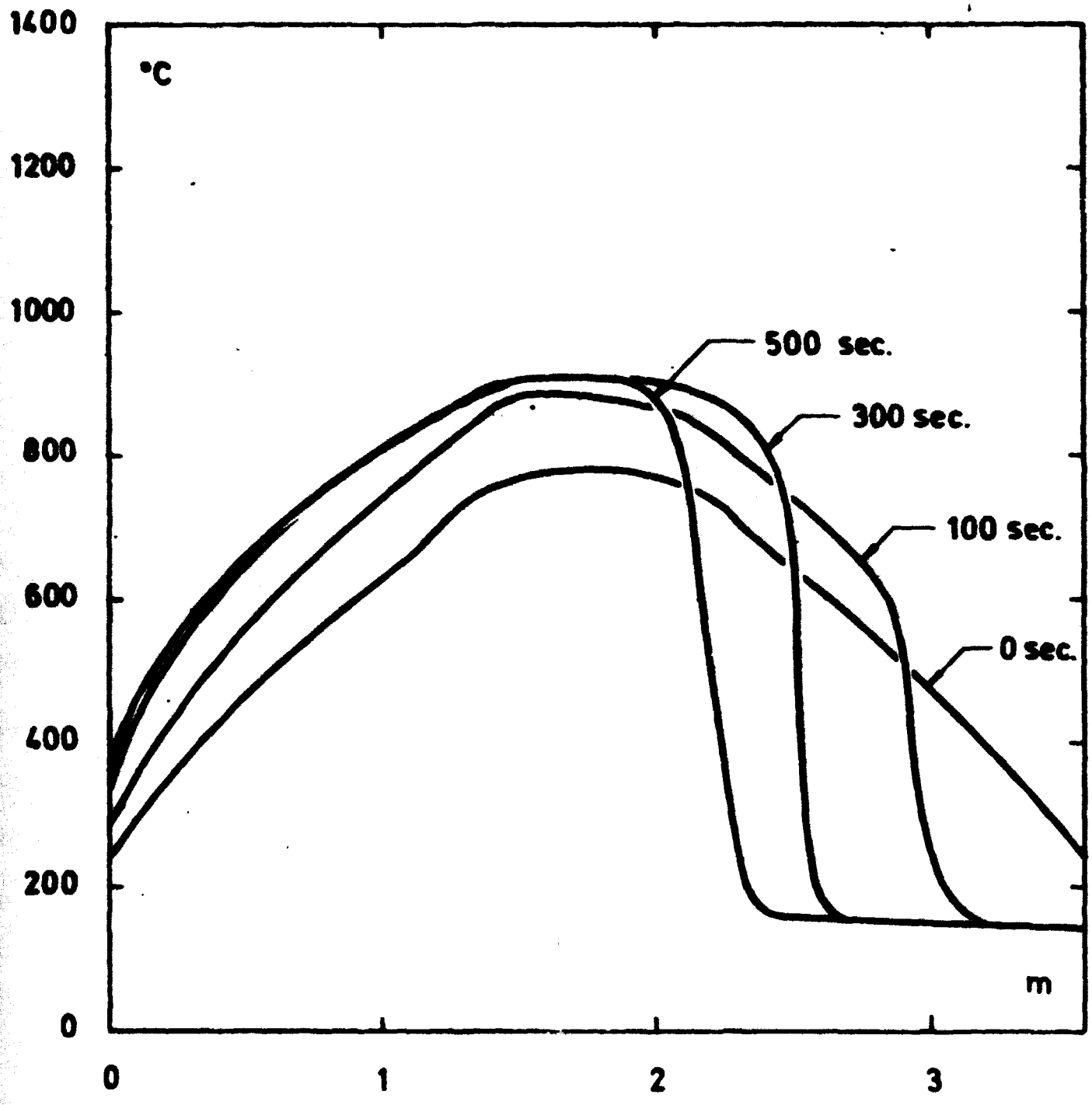

Fig. 4.11. BWR - FLECHT run 5x. Temperature profiles for group 3.

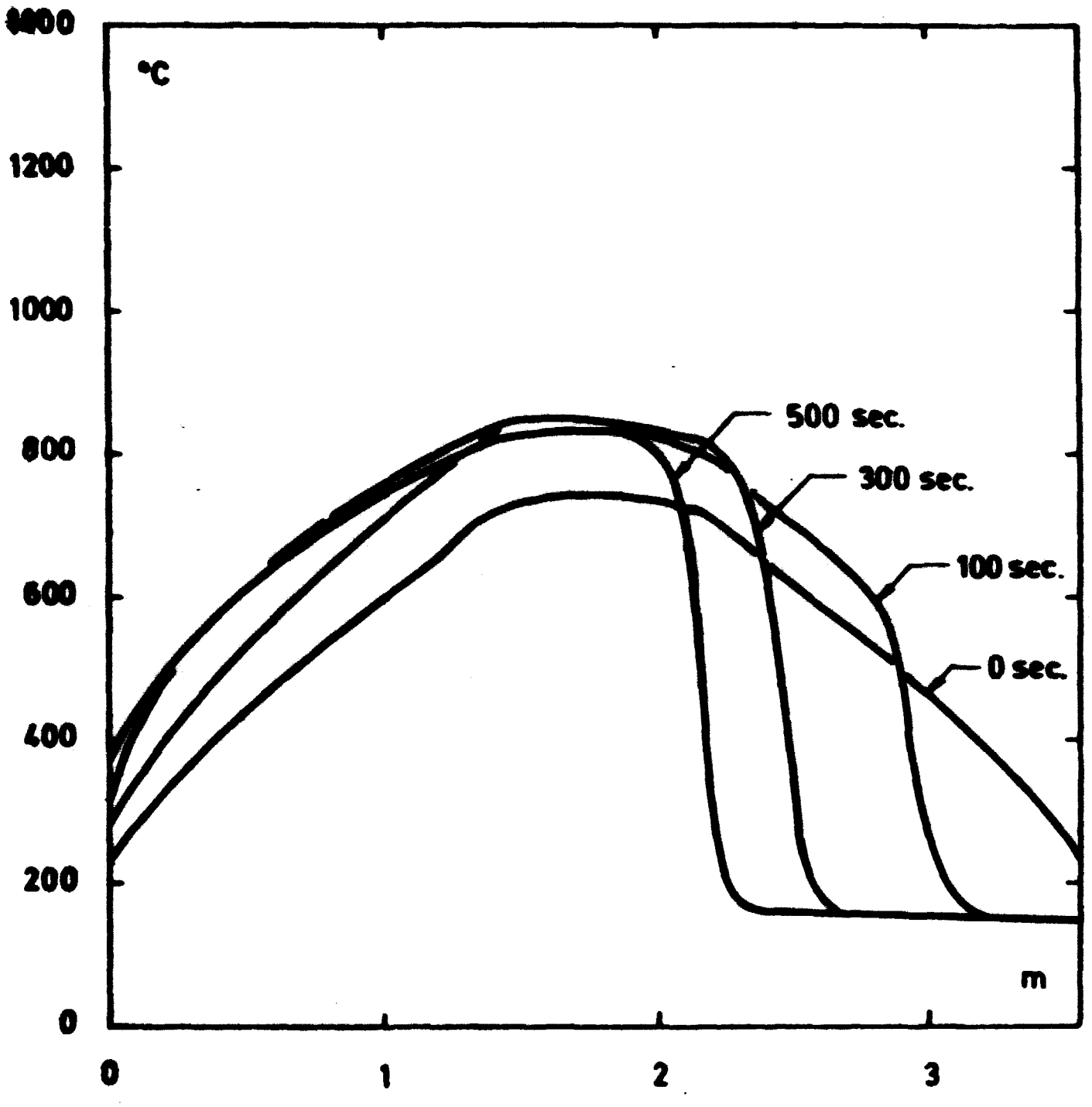

Fig. 4.12. BWR – FLECHT run 5x. Temperature profiles for group 4.

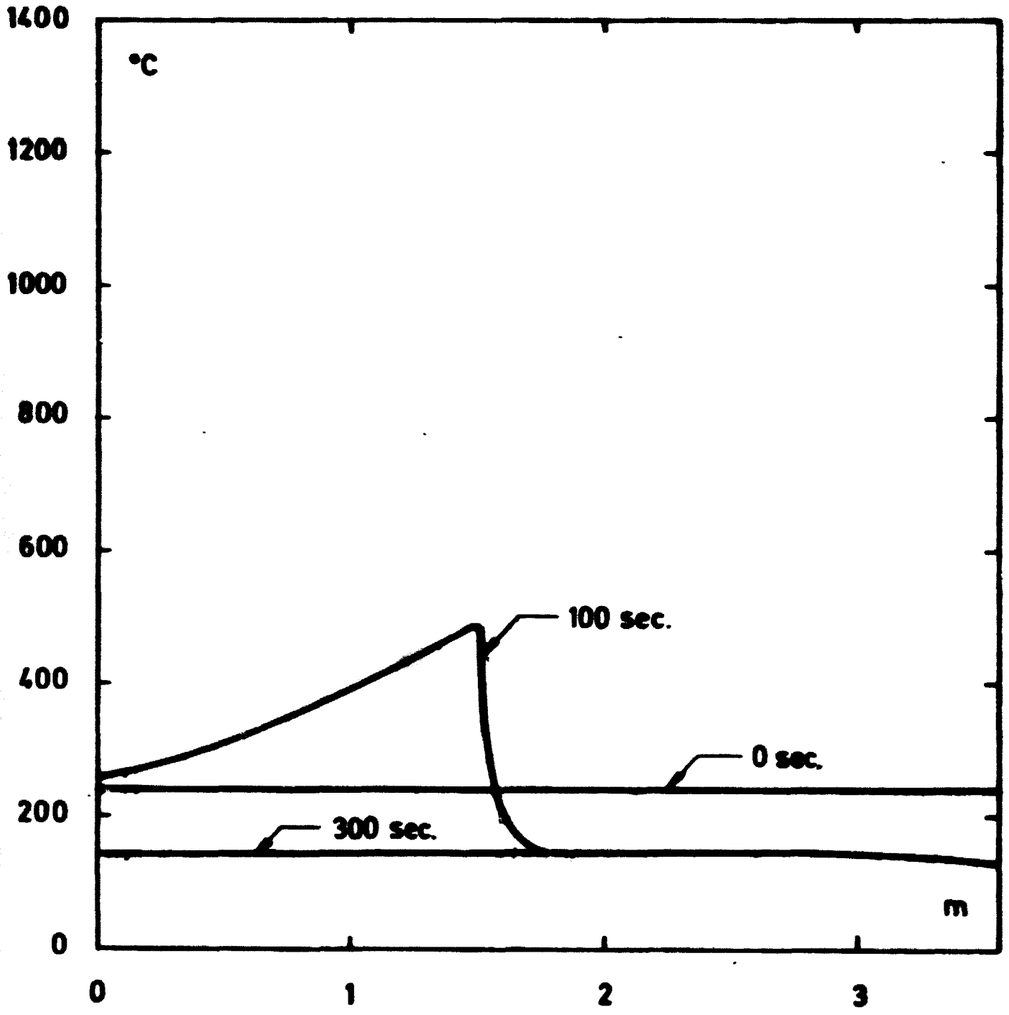

Fig. 4.13. BWR - FLECHT run 5x. Temperature profiles for shroud.

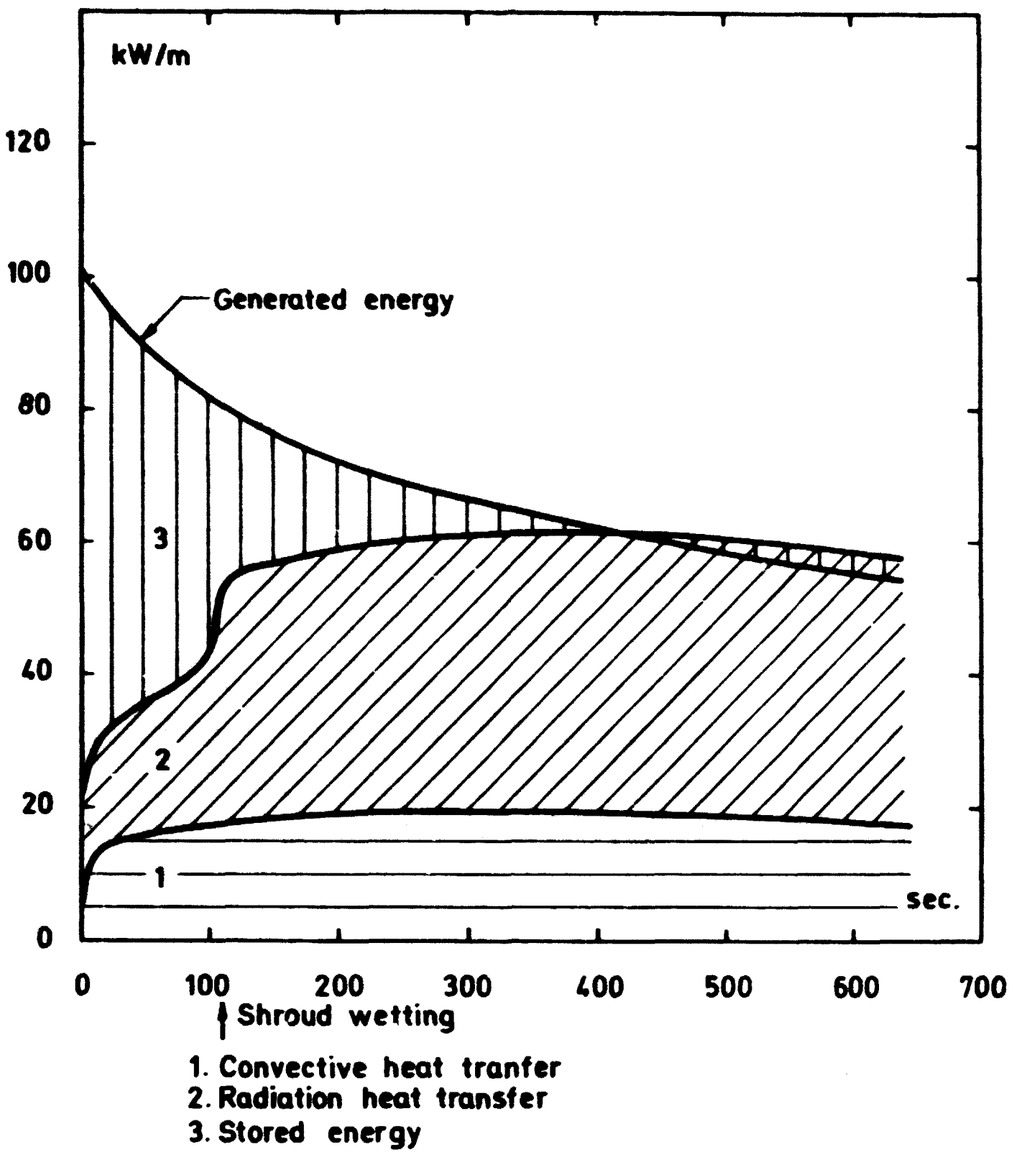

Fig. 4.14. Energy balance at midplane for BWR - FLECHT fuel element, run 5x.

In fig. 4.14 is for run 5x shown how the energy generated at the bundle midplane in all the rods is shared between convective and radiation heat transfer and stored energy in the rods. Figs. 4.15 and 4.16 show the same for run 5x, but for a single rod in group 1 and group 4, and it is seen that thermal radiation is more dominant for a rod close to the shroud than for a central rod.

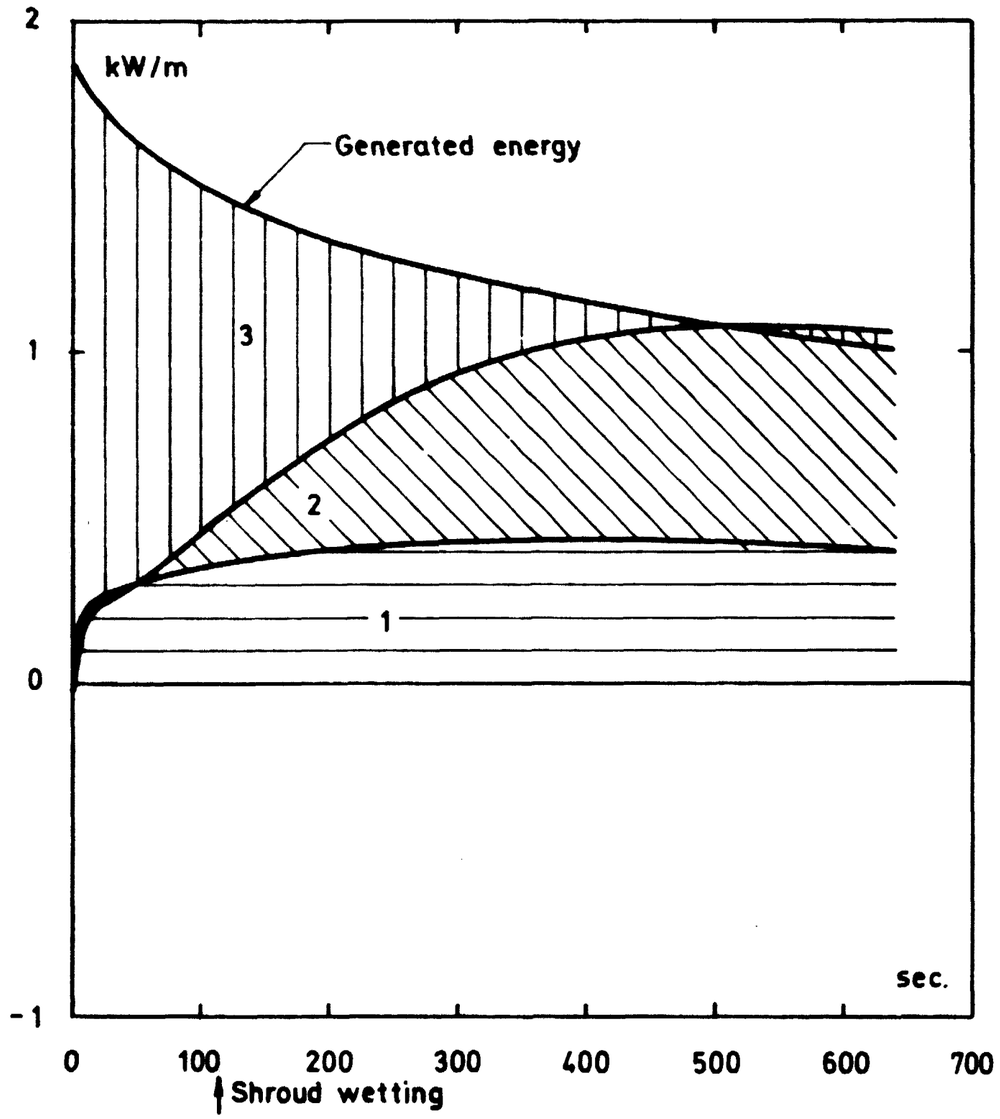

1. Convective heat transfer
2. Radiation heat transfer
3. Stored energy

Fig. 4.15. Energy balance at midplane for BWR - FLECHT fuel rod in group 1, run 5x.

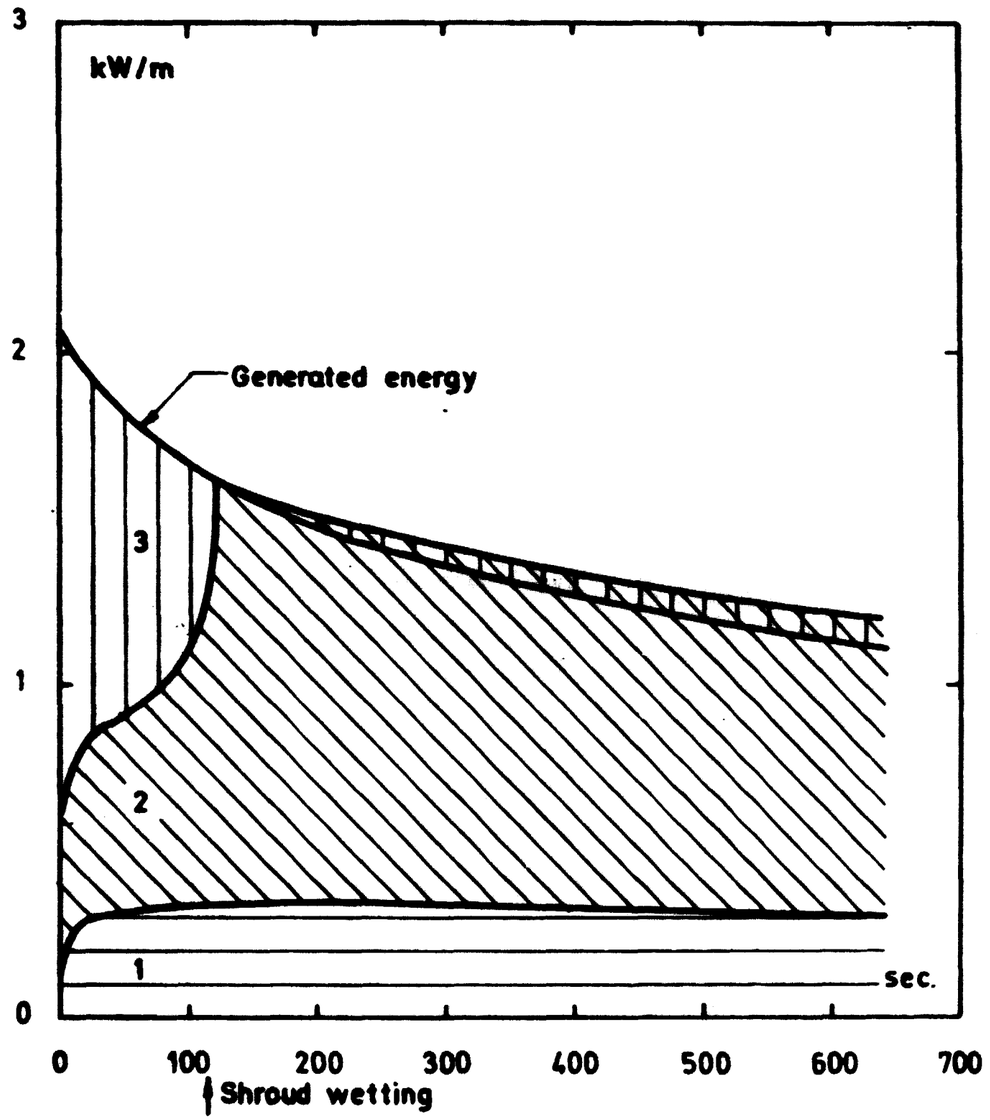

1. Convective heat transfer
2. Radiation heat transfer
3. Stored energy

Fig. 4.16. Energy balance at midplane for BWR - FLECHT fuel rod in group 4, run 5x.

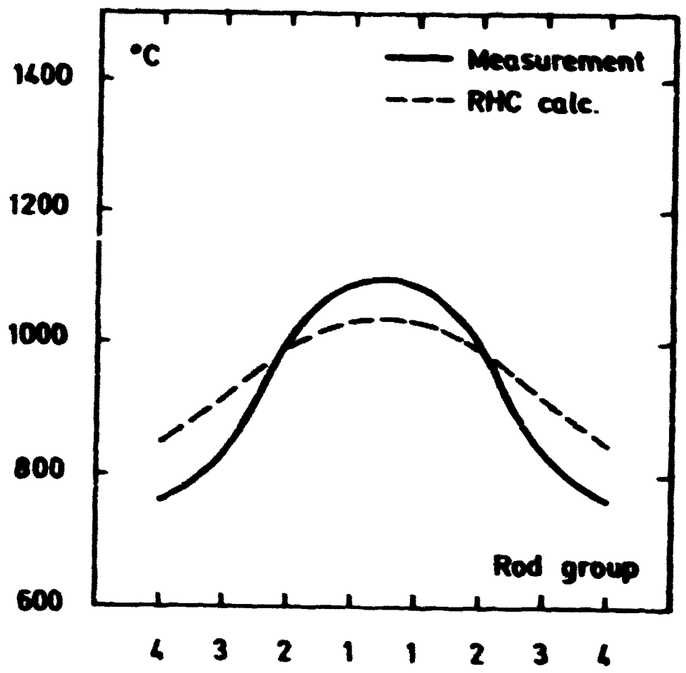

Fig. 4.17. BWR-FLECT run 5x. Max. temperatures.

The wetting times for the shroud and some of the rods are measured, and in tables 4.5 and 4.6 is given a comparison between the measured and the calculated wetting times. It is seen that the agreement is very good although the model overpredicted the wetting time of the shroud for runs 4 and 5x by a factor of 2 to 3. The overprediction of these wetting times is mainly due to uncertainties about the initial shroud temperature, which was known only at the midplane.

As stated in subsection 3.3.1 thermal non-equilibrium should be less marked at high pressures. This is due to the fact that with increasing steam density the slip will decrease and the droplet concentration increase, and thus the net heat transfer between the droplets and the steam will increase. This effect is further increased as higher steam densities mean higher Weber numbers, and consequently smaller droplets. In table 4.7 are shown the steam superheat, the droplet size, the slip, the droplet concentration, and the droplet subcooling at the 0.65 m elevation, where for the BWR-FLECHT calculations the maximum superheat occurs, and at t = 500 seconds where the temperature is at maximum (cf. figs. 4.5 - 4.8). The figures in table 4.7 do not agree completely with the above-mentioned arguments; this is to some extent due the lack of equilibrium with respect to both energy and momentum, but is mainly due to different positions of

Table 4.5

Wetting time at fuel element midplane, upper value calculated and lower value measured

Run	Pressure bar	Group 2 sec.	Group 3 sec.	Shroud sec.
4	2.07	—— x) 1680 xx)	—— 1320 +)	65 25
5x	4.14	—— ——	—— 720	70 25
6	6.205	——	610 510	14 10
8(2)	13.79	460 500	460 310	10 25

x) Measurement not recorded or transient not calculated until the occurrence of wetting.
xx) Average for rods 9, 10, and 11.
+) Rod 2.

Table 4.6

Wetting times at 2.75 m elevation, upper value calculated and lower value measured

Run	Pressure bar	Group 2 sec.	Group 3 sec.
4	2.07	510 —— x)	530 530 +)
5x	4.14	290 ——	290 290
6	6.205	220 ——	220 190
8(2)	13.79	140 180 xx)	150 120

x) Measurement not recorded.
xx) Average for rods 9, 10, and 11.
+) Rod 2.

Table 4.7

Superheat, droplet size, slip, droplet concentration, and droplet subcooling at 0.65 m elevation at t = 500 seconds

Run	4	5x	6	8(2)
Pressure, bar	2.07	4.14	6.205	13.79
Saturation temp., ^{o}C	121	145	160	194
Superheat, ^{o}C	283	194	148	100
Droplet diameter, m	$2.14 \cdot 10^{-3}$	$2.41 \cdot 10^{-3}$	$3.01 \cdot 10^{-3}$	$1.64 \cdot 10^{-3}$
$v_{droplet} - v_{steam}$, m/sec.	1.09	-1.70	-2.84	-2.33
Droplet concentration	$1.05 \cdot 10^{-3}$	$0.83 \cdot 10^{-3}$	$0.63 \cdot 10^{-3}$	$0.91 \cdot 10^{-3}$
Droplet subcooling, ^{o}C	7.1	12.9	19.4	1.8

the wetting fronts on the rods (cf. tables 4.5 and 4.6), causing a difference between the amounts of droplets originating directly from the spray system and/or from sputtering in a film front. Droplets originating directly from the spray system will be subcooled, while droplets from sputtering will have the saturation temperature, and as the wetted part of the rods increases, the evaporation from the film increases too, and the number of droplets produced on account of sputtering decreases. Furthermore the droplets produced by sputtering are generally smaller than the droplets coming directly from the spray system.

However, it is clearly seen that the superheat of the steam decreases with increasing pressure.

4.3. Conclusions from the BWR-FLECHT Calculations

From the comparison of the RHC calculations with the BWR-FLECHT experimental results the following conclusions can be drawn:

1. The computer code RHC is able to predict the maximum cladding temperature with an error of generally less than $60^{o}C$.

2. RHC is able to predict the wetting times for both the shroud and the rods, generally with an error of generally less than 30 seconds.
3. Of the heat transfer from all the rods about $\frac{1}{3}$ is due to convection and about $\frac{2}{3}$ to thermal radiation. Generally the thermal radiation is more dominant for the outer rods, and less dominant for the central rods.
4. The steam will be superheated by 100 - $300^{o}C$, and the superheat will decrease with increasing pressure. Consequently a heat sink at the saturation temperature cannot be used for the convective heat transfer.
5. As the pressure increases, the maximum temperature will decrease. This is mainly due to the smaller rewetting times with increasing pressure.

5. BWR/6 CALCULATIONS

A core heat-up and emergency core cooling transient was calculated for a BWR/6-238 reactor[28]. The calculation was made as a demonstration of the capability of the model.

Again a number of assumptions had to be made, mainly concerning the initial temperature distribution and the emergency core spray cooling. Many data must be considered as typical for that reactor, e.g. the temperature distribution at the end of blow-down, and they have not been chosen on a conservative basis. Consequently the calculations must not be considered as a safety analysis for a BWR/6 reactor, but merely as a typical transient for that reactor. However, some conclusions can be drawn from the BWR/6 calculation, and one of the most essential is that flow stagnation is likely to occur somewhere in the fuel element.

5.1. Description of the BWR/6-238

The BWR/6-238 reactor is described in reference 28. The most essential changes compared with previous reactors are the introduction of an 8x8 fuel element with 63 fuel rods and one water rod (cf. fig. 5.2), and a reduction of the power peaking and the linear power. Furthermore the effective length of the fuel elements and the number of fuel elements have been increased.

For the same size of reactor vessel the net power output is increased by 20% in comparison with the BWR/5, and an increase in the safety margins is postulated. The main data of the BWR/6-238 are given in table 5.1. The material properties of UO_2 and Zr are given in table 5.2. In figs. 5.1 and 5.2 are shown the axial power profile and the local power peaking, and in fig. 5.3 the relative power versus the time after the accident. The decay heat is based on the ANS-standard[6]. The local power peaking for the 7-rod-group model (cf. fig. 5.2) used in the calculations is shown in table 5.3.

Table 5.1

Main data of the BWR/6-238

Nominal thermal power, W	$3.579 \cdot 10^9$
Electrical power, W	$1.250 \cdot 10^9$
Thermal power used in the calculation = 1.02 x nominal power, W	$3.651 \cdot 10^9$
Number of fuel elements	732
Radial power peaking	1.4
Axial power peaking	1.4
Local power peaking	1.13
Total power peaking	2.22
Active core height, m	3.759
Number of fuel rods per element	63
Fuel rod outside diameter, m	$1.252 \cdot 10^{-2}$
Cladding thickness, m	$0.866 \cdot 10^{-3}$
Fuel pellet diameter, m	$1.057 \cdot 10^{-2}$
Fuel rod spacing, m	$1.626 \cdot 10^{-2}$
Fuel element inside dimension, m	$1.341 \cdot 10^{-1}$
Shroud thickness, m	$3.048 \cdot 10^{-3}$
Spray water flow per bundle, kg/sec.	$1.986 \cdot 10^{-1}$ ⁎)
Spray water temperature °C	85.0 +)
Containment pressure after blow-down, bar	3.5 +)
Emissivity of ZrO_2	0.67
Emissivity of water	0.96

⁎) Corresponds to 3.25 gpm[29].

+) Assumed value.

Table 5.2

Material properties of UO_2, Zr, and ZrO_2[15, 8])

	Density kg/m³	Heat capacity J/kg °C	Thermal conductivity W/m °C
UO_2	$1.028 \cdot 10^4$	$3.267 \cdot 10^2 + T(-4.518 \cdot 10^{-2} + T \cdot 3.72 \cdot 10^{-5}$ ⁎)	$7.020 + T(-6.387 \cdot 10^{-3} + T \cdot 2.114 \cdot 10^{-6})$
Zr	$6.40 \cdot 10^3$	$2.605 \cdot 10^2 + T(1.789 \cdot 10^{-1} - T \cdot 6.549 \cdot 10^{-5}$	$1.561 \cdot 10^1 + T(-3.357 \cdot 10^{-3} + T \cdot 1.375 \cdot 10^{-5})$
ZrO_2	$5.60 \cdot 10^3$	$6.2 \cdot 10^2$	2.6

⁎) T is the temperature, °C.

Table 5.3

Local power peaking in 7 group model

Group	No. of rods	Local power peaking
1	1	0.0 x)
2	8	0.942
3	7	0.919
4	16	1.005
5	4	0.390
6	16	1.124
7	12	1.116

x) Group 1 is the water rod.

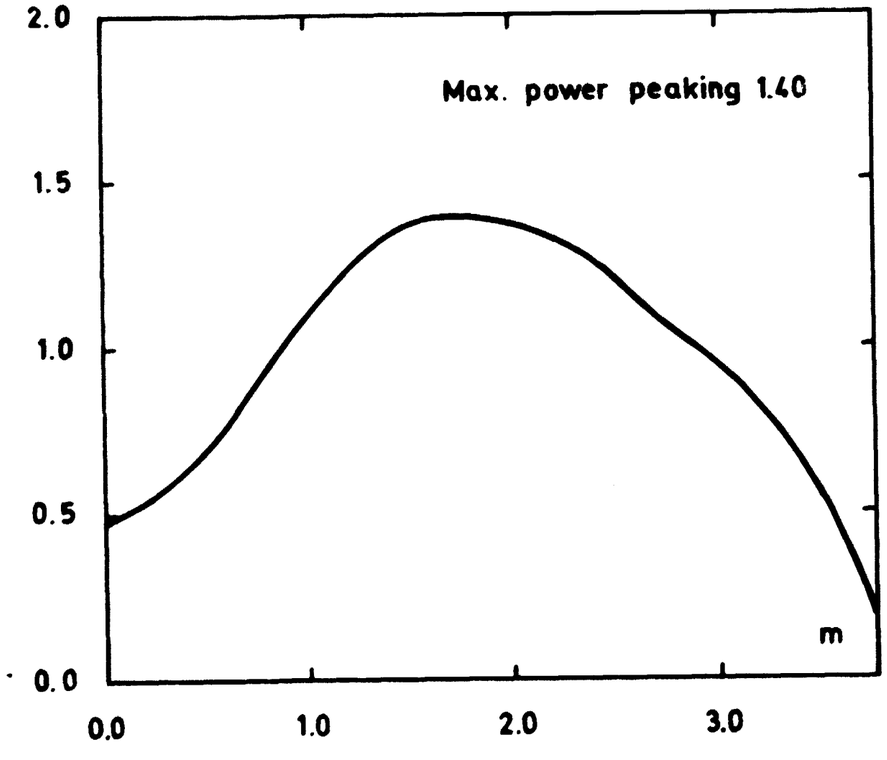

Fig. 5.1 Axial power profile BWR/6 fuel element.

1 1.09 7	2 1.12 7	3 1.13 6	4 1.11 6	5 1.12 6	6 1.13 6	7 1.12 7	8 1.10 7
9 1.12 7	10 0.39 5	11 0.99 4	12 1.01 4	13 1.01 4	14 0.99 4	15 0.39 5	16 1.13 7
17 1.13 6	18 0.99 4	19 0.91 3	20 0.92 3	21 0.92 3	22 0.92 3	23 0.99 4	24 1.13 6
25 1.11 6	26 1.01 4	27 0.92 3	28 0.90 2	29 0.93 2	30 0.94 2	31 1.02 4	32 1.12 6
33 1.12 6	34 1.01 4	35 0.92 3	36 0.93 2	37 0.00 1	38 0.97 2	39 1.03 4	40 1.12 6
41 1.13 6	42 0.99 4	43 0.92 3	44 0.94 2	45 0.97 2	46 0.95 2	47 1.00 4	48 1.13 6
49 1.12 7	50 0.39 5	51 0.99 4	52 1.02 4	53 1.03 4	54 1.00 4	55 0.39 5	56 1.13 7
57 1.10 7	58 1.13 7	59 1.13 6	60 1.12 6	61 1.12 6	62 1.13 6	63 1.13 7	64 1.10 7

Fig. 5.2. Rod numbers, lokal power peaking, and rod groups for BWR/6 fuel element.

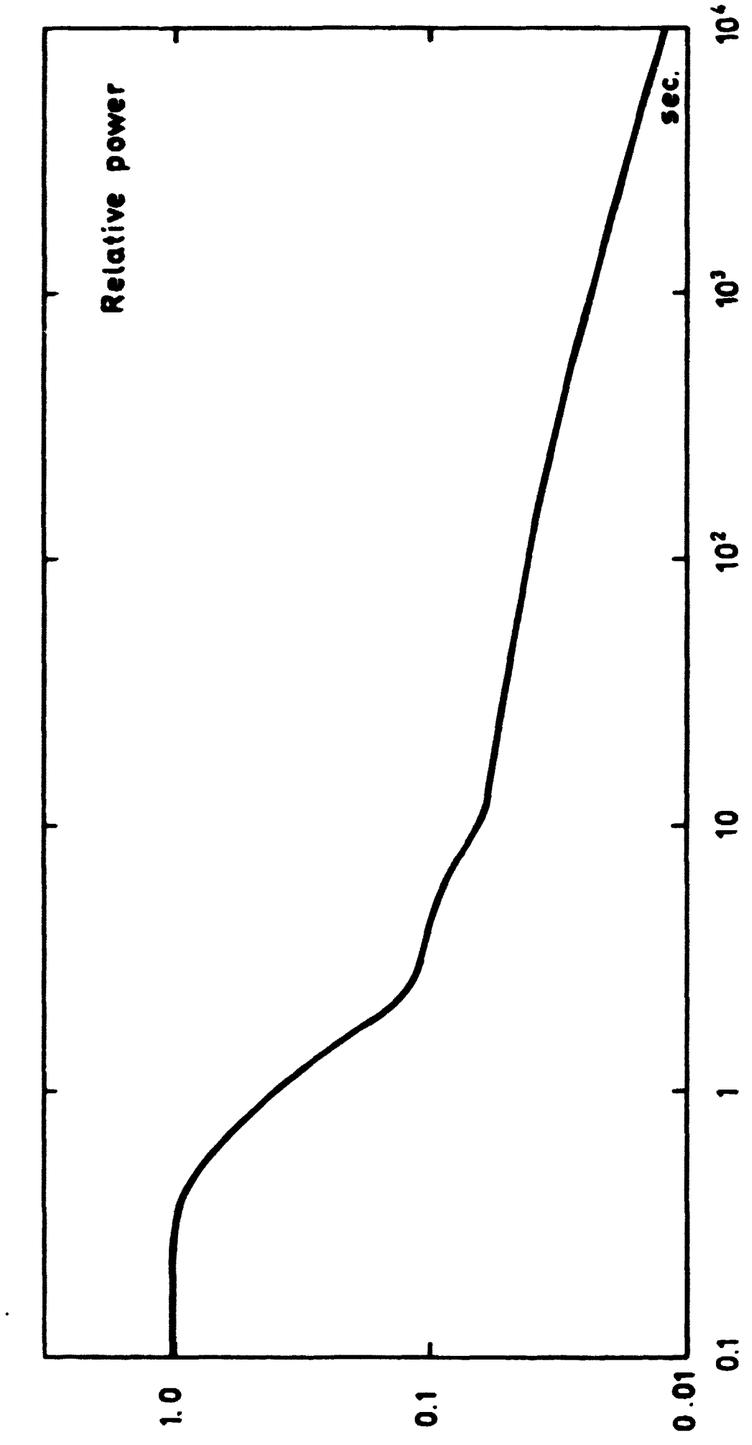

Fig. 5.3. Relative power of BWR/6 - 238.

5.2. RHC Calculations on the BWR/6-238

A calculation of a core heat-up and emergency core cooling transient for the highest powered fuel element was made for the BWR/6. Only one of the two spray systems was assumed to be in operation, and the spray flow rate was assumed to be the minimum guaranteed flow rate[29] (cf. table 5.1). In table 5.4 are shown the maximum temperatures for the different rod groups and the shroud, and in fig. 5.4 the temperature transients for the 1.72 m elevation, where the maximum temperature of the rods occurs.

Table 5.4

Maximum temperatures for the BWR/6 element

Rod group No.	Max. temp. °C	Elevation m	Time sec.
1	1103	1.72	350
2	1153	1.72	350
3	1137	1.72	350
4	1110	1.10	370
5	1050	1.10	370
6	1091	1.10	350
7	1076	1.10	350
Shroud	1008	1.10	350

From fig. 5.1 and table 5.4 it is seen that for the central rods the maximum temperature occurs where the power is at maximum, whereas the maximum temperature for the outer rods occurs at a somewhat lower position. This is due to the slow propagation of the film front. The water rod (rod group 1) is seen to follow the temperatures of the neighbouring rods very closely, and within 200 seconds it reaches a level of about 1000 - 1100°C. This is mainly due to the high intensity of thermal radiation in the centre of the element and the low heat capacity of the rod. The rapid temperature increase of the water rod will cause a delay in the rewetting of the rod, and the rewetting time of the water rod is more likely to follow the rewetting of fuel rods than that of the shroud. This is also seen in fig. 5.5, where the film front position is shown versus the time.

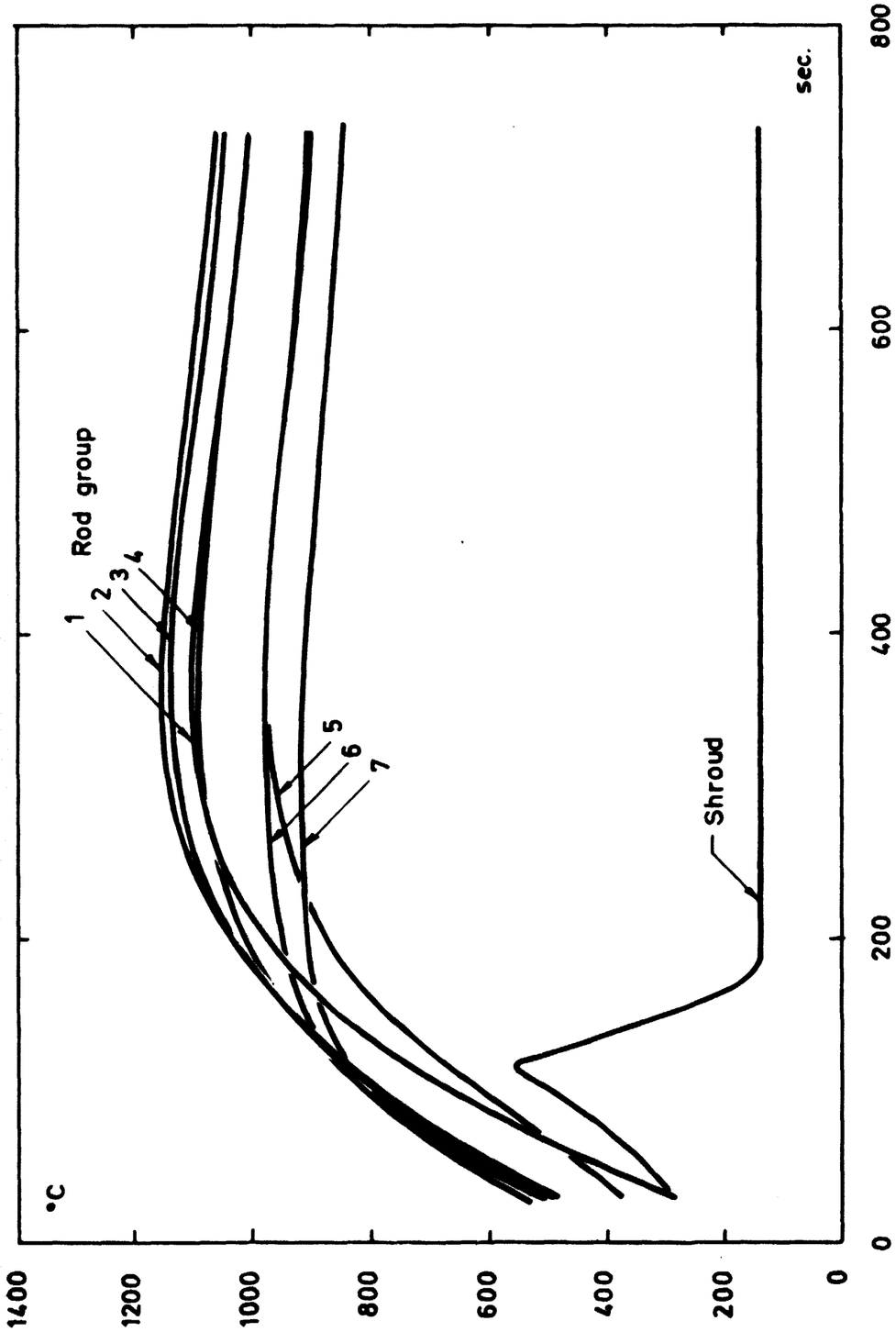

Fig. 5.4. BWR /6 - 238. Temperatures at 1.72 m elevation.

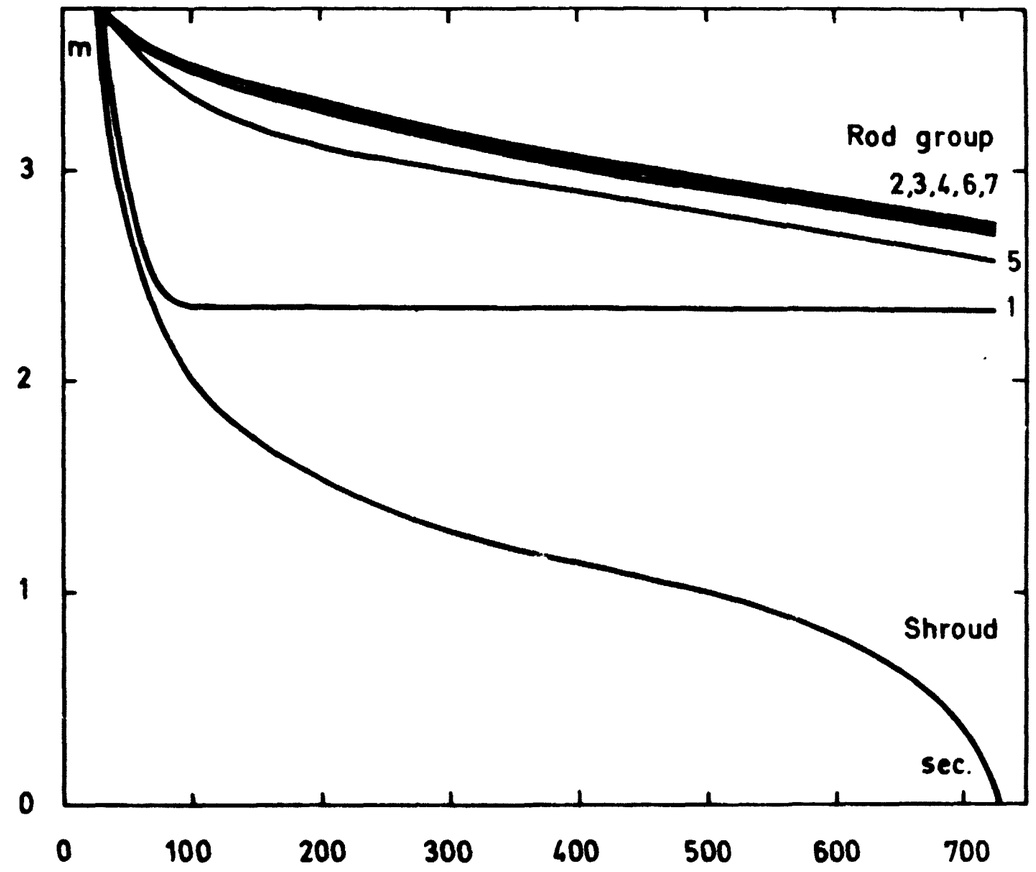

Fig. 5.5. BWR / 6 - 238. Position of film front.

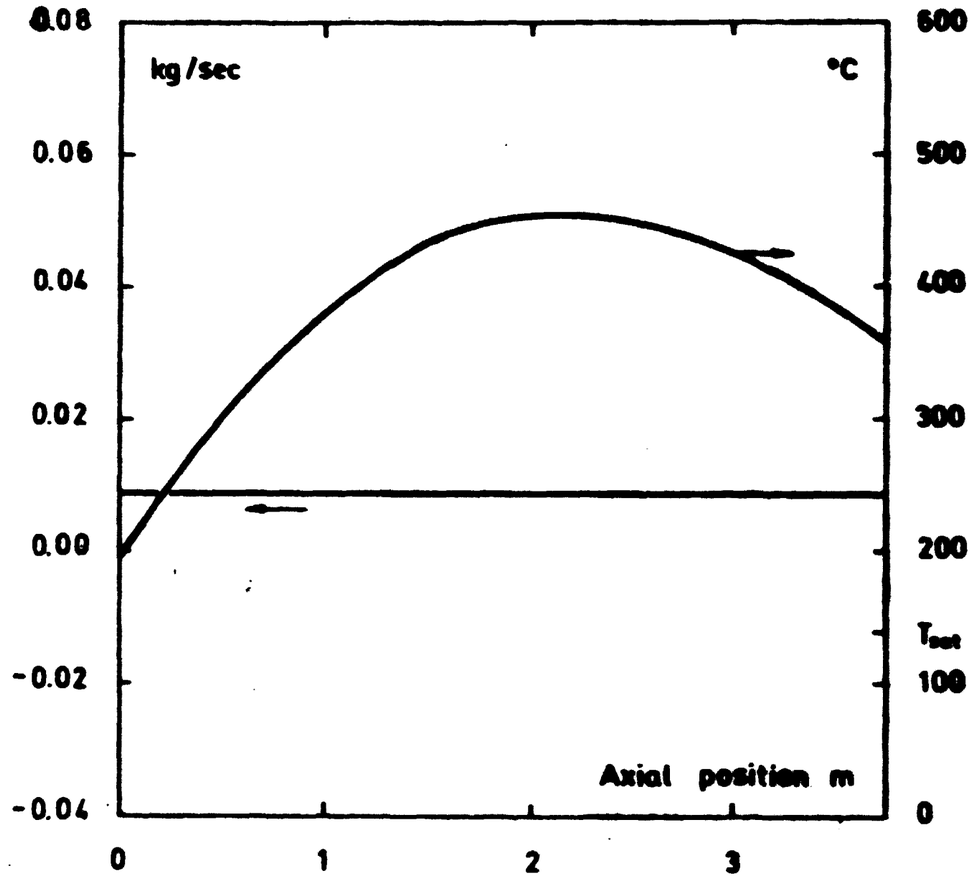

Fig. 5.6. Steam flow in a BWR/6 fuel element at t = 30 seconds.

In figs. 5.6 - 5.9 are shown the steam flow and temperatures in the fuel element at 30, 270, 490, and 730 seconds after the accident. The steam flow at 30 seconds is due to boiling in the lower plenum, while later the steam flow is due to evaporation of emergency core coolant in the fuel element. Flow stagnation is observed at a point approximately $\frac{1}{3}$ above the bottom of the fuel, this point is of course dependent on the flow resistance in the primary system.

Furthermore it is seen that the steam superheat is likely to be in the order of 100 - 300°C. The dip observed in figs. 5.7 and 5.8 is due to the boiling and consequent production of saturated steam in the film front at the shroud (cf. fig. 5.5).

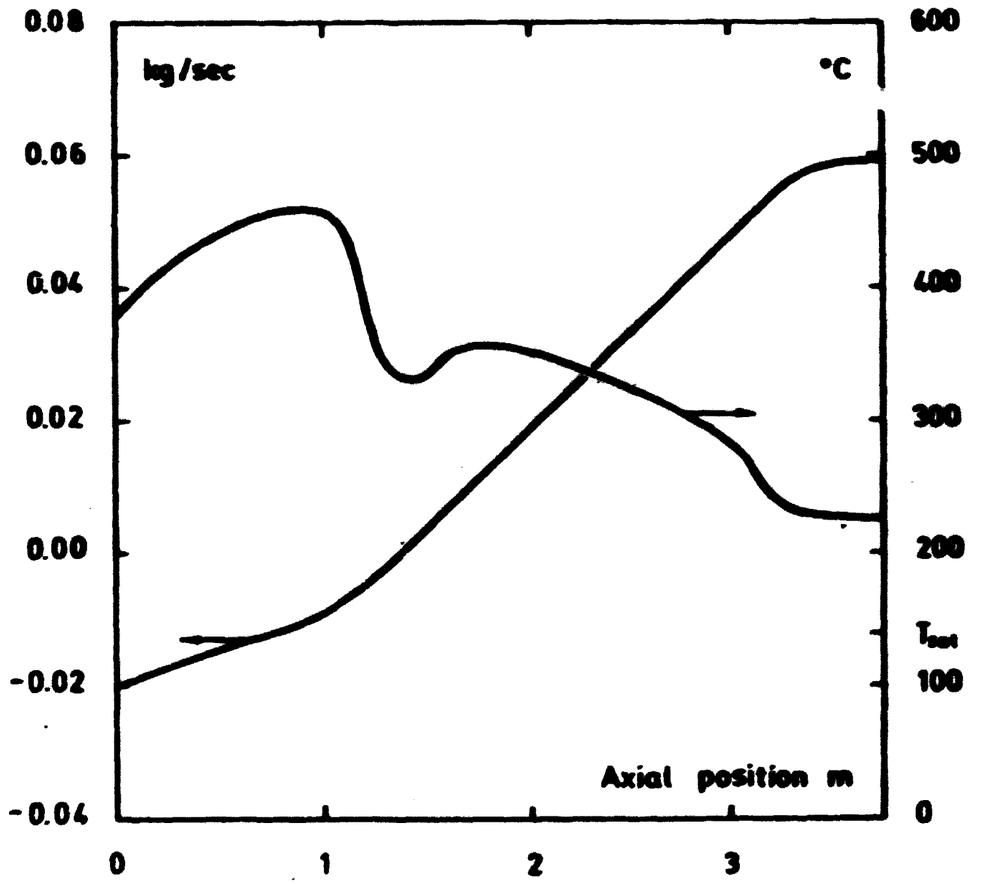

Fig. 5.7. Steam flow in a BWR/6 fuel element at t = 270 seconds.

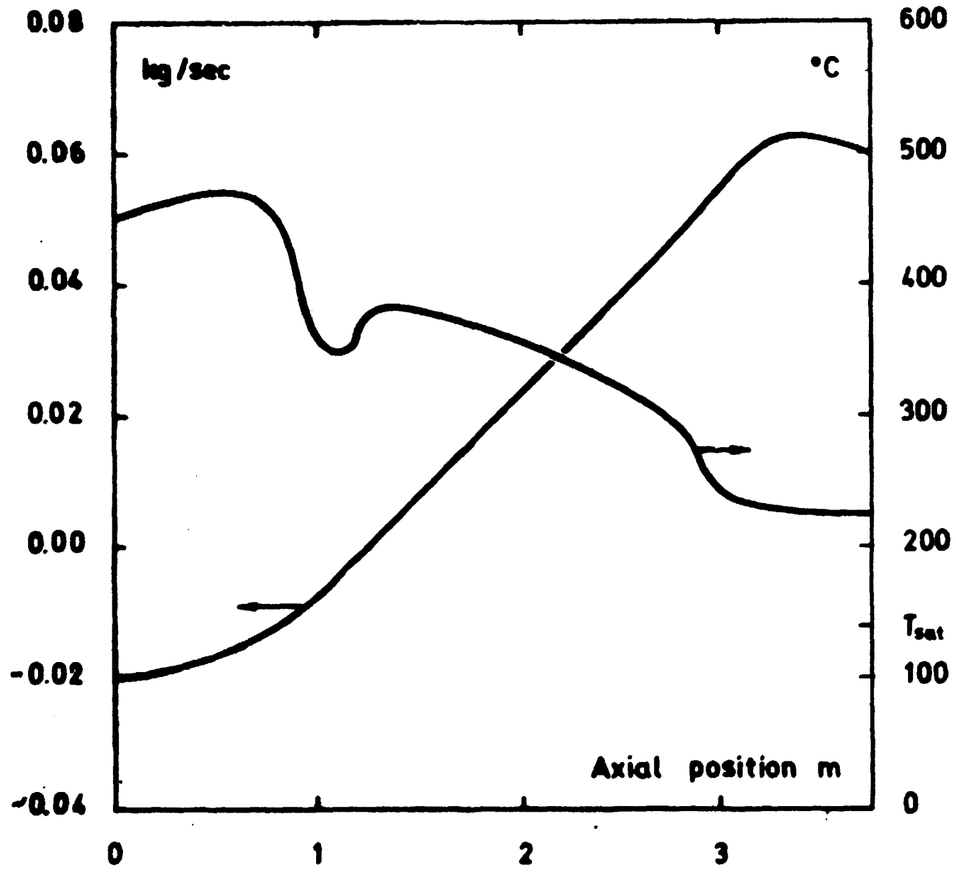

Fig. 5. 8. Steam flow in a BWR/6 fuel element at t=490 seconds.

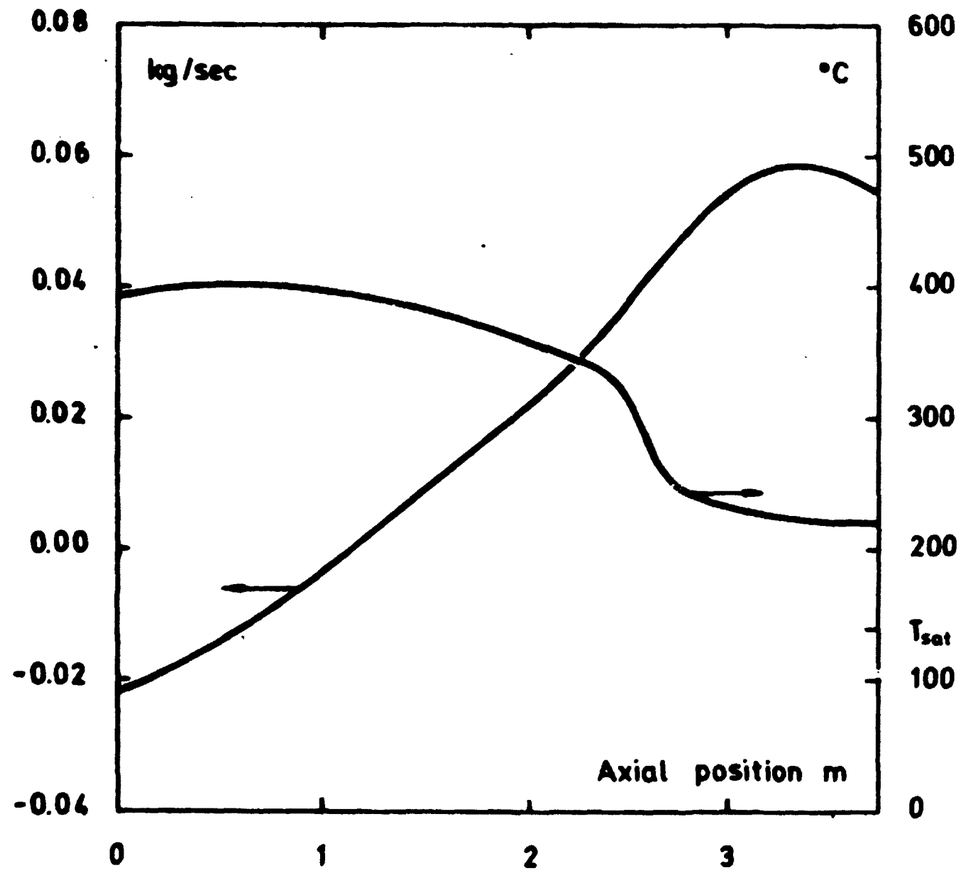

Fig. 5. 9. Steam flow in a BWR/6 fuel element at t=730 seconds.

Fig. 5.10 shows the metal-water reaction and the release of hydrogen.

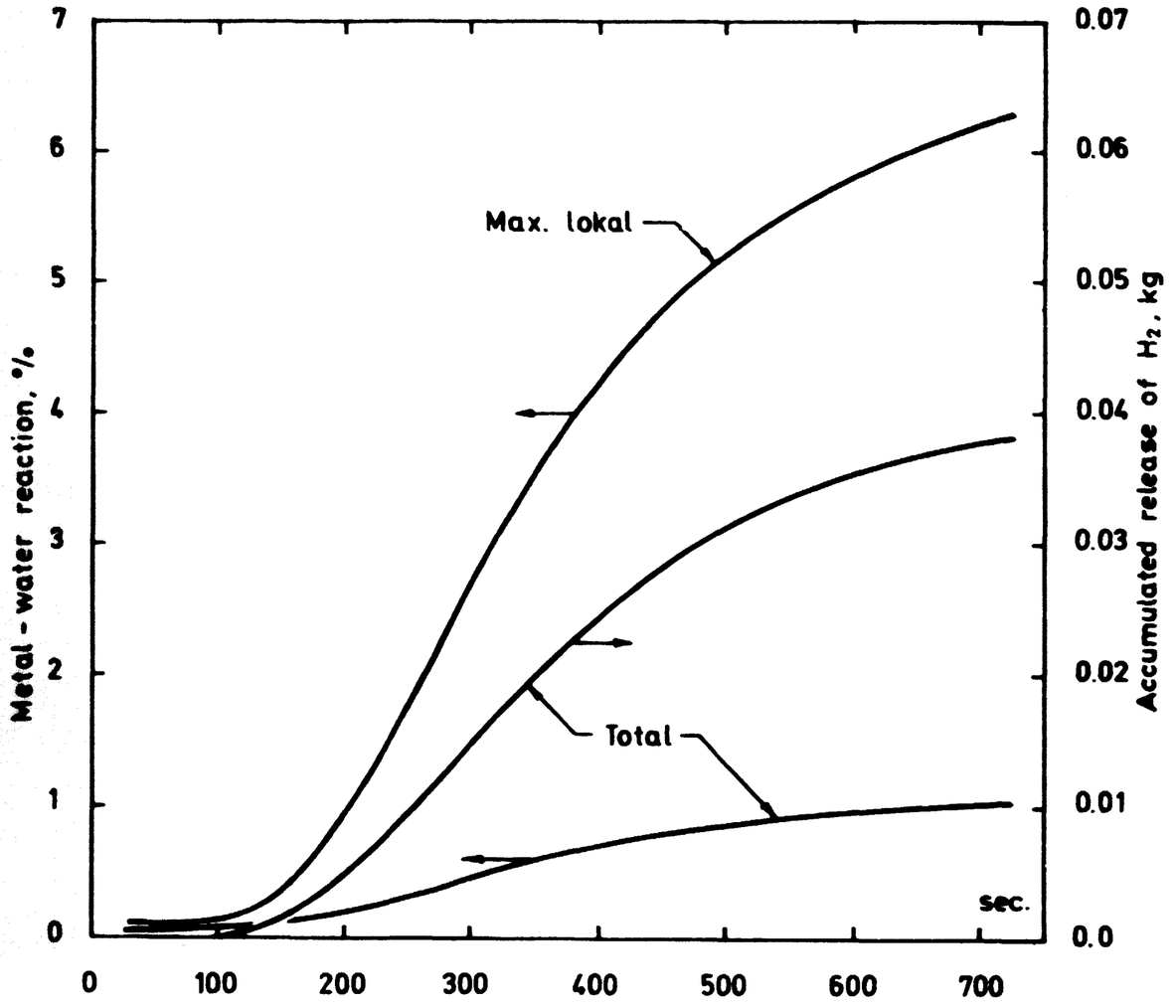

Fig. 5.10. BWR/6 - 238. Metal - water reaction.
Max. lokal reaction at rod group 2 and 1.72 m elevation.

5.3. Conclusions from the BWR/6 Calculations

From the result of the calculation on the BWR/6-238 fuel element the following conclusions can be drawn:

1. Flow stagnation is likely to occur somewhere in the fuel element, dependent on the flow resistance in the primary system.

2. The influence of the water rod on the core heat-up and emergency core cooling transient is minor, i. e. the wetting time of the water rod is of the same order as the wetting time of the fuel rods.
3. The amount of metal-water reaction is in the order of a few per cent.
4. The maximum temperatures occur later than the wetting of the shroud, and they are likely to occur somewhat below the point of peak power.

6. DISCUSSION AND CONCLUSIONS

Although the model RHC has proved quite useful in the accident analysis of nuclear power reactors and especially in the sophisticated analysis of heat transfer and two-phase flow, it should be recognized that further development of several aspects of the model is desirable. The present version of RHC contains a detailed description of the physical and chemical phenomena appearing in core heat-up and emergency core spray cooling transients, but it is based on a rather simple geometrical model. This indicates two main areas of further development, namely the development of models for the physical phenomena involved in flooding transients, and the inclusion of a more detailed description of the primary system, i. e. several parallel fuel channels, bypass channels, several external loops, etc. Furthermore a model for the coupling to fuel rod failure is desirable.

Minor improvements in the models of the present version of RHC may also be considered. A transport correction of the radiation heat transfer to account for anisotropic scattering has already been suggested, but the model of rewetting of hot surfaces by falling films[22] may be improved, too. Finally and especially in connection with accident analysis on PWR's it might turn out to be necessary to include sub-channel analysis in the model.

However, on the basis of the comparison with the BWR-FLECHT and the BWR/6 calculation some main conclusions can be drawn. A steam superheat in the order of 100 - 300°C will exist, and flow stagnation in the fuel element is likely to occur, and this in connection with the fact that about one third of the heat is removed from the fuel on account of convection necessitates the high degree of sophistication of RHC. And it should be noted from the BWR-FLECHT comparison that the model is able to calculate both the temperatures and the rewetting with a high degree of accuracy, the maximum temperatures e. g. are calculated to within 60°C, and the wetting times generally to within 30 seconds.

All things considered it must be concluded that the model, RHC, is able to perform a detailed analysis of the temperature distribution, the heat transfer, and two-phase flow for a core heat-up and emergency core cooling transient, and in connection with suitable models for fuel rod failures and the release and transport of fission products RHC is an effective tool in the safety evaluation of a nuclear power reactor.

7. ACKNOWLEDGEMENT

The author gratefully acknowledges the assistance of the entire staff of the Reactor Physics Department at Risø and especially thanks A. Olsen and H. Abel-Larsen for several valuable discussions.

8. REFERENCES

1) F.R. Farmer, Siting Criteria - A New Approach. In: Containment and Siting of Nuclear Power Plants. Proceedings of a Symposium held 3-7 April 1967 (IAEA, Vienna, 1967) 303-324.

2) Concluding Statement of Position of the Regulatory Staff, Acceptance Criteria for Emergency Core Cooling for Light-Water Cooled Nuclear Power Reactors. Docket-RM-50-1 (1973) 222 pp.

3) C. Star, M.A. Greenfield, and D.F. Hausknecht, A Comparison of Public Health Risks: Nuclear vs. Oil-fired Power Plants. Nucl. News, 15 No. 10 (1972) 37-45.

4) G.D. Bell, Methods for the Evaluation of Risk. Paper presented at Reactor Safety Course No. 12, Harwell, 5-30 June 1972. 8 pp. Unpublished.

5) J. Andersen and H. Abel-Larsen, REMI/HEAT COOL, a Computer Programme for Calculation of Core Heat Up with Spray Cooling. Risø-M-1541 (1972) 29 pp.

6) Proposed ANS Standard, Decay Energy Release Rates following Shutdown of Uranium-fueled Thermal Reactors, Approved by Subcommittee. ANS-5.1 (1971) 7 pp.

7) L. Baker and L.C. Just, Studies of Metal-Water Reactions at High Temperatures. ANL-6548 (1962) 86 pp.

8) J.C. Hesson, J.L. Anderson, and R.O. Ivins, CHEMLOC - II: A Computer Program Describing the Core Heating and Cladding - Steam Reaction for a Water-Cooled Power Reactor following a Loss of Coolant. ANL-7361 (1968) 115 pp.

9) A. Yamanouchi, Effect of Core Spray Cooling in Transient State after Loss of Coolant Accident. J. Nucl. Sci. Technol. (Tokyo) 5 (1968) 547-558.

10) J.D. Duncan and J.E. Leonard, BWR Standby Cooling Heat Transfer Performance under Simulated Loss-of-Coolant Conditions between 15 and 300 psia. GEAP-13190 (1971) 220 pp.

11) J.D. Duncan and J.E. Leonard, Emergency Cooling in Boiling Water Reactors under Simulated Loss-of-Coolant Conditions. BWR-FLECHT Final Report. GEAP-13197 (1971) 86 pp.

12) L.S. Tong, Boiling Heat Transfer and Two-Phase Flow (Wiley, New York, 1965) 242 pp.

13) P.N. Rowe, K.T. Claxton, and J.B. Lewis, Heat and Mass Transfer from a Single Sphere in an Extensive Flowing Fluid. Trans. Inst. Chem. Eng. 43 (1965) T14-T31.

14) E.M. Sparrow and R.D. Cess, Radiation Heat Transfer (Brooks/Cole, Belmont, Calif., 1970) 340 pp.

15) B.C. Slifer and J.E. Hench, Loss-of-Coolant Accident and Emergency Core Cooling Models for General Electric Boiling Water Reactors. NEDO-10329 (1971) 239 pp.

16) G.B. Wallis, One-dimensional Two-phase Flow (McGraw-Hill, New York, 1969) 408 pp.

17) Lord S. Rayleigh, On the Instability of Jets. Proc. Lond. Math. Soc. 10 (1878/79) 4-13.

18) R. de Vogelaere, A Method for Numerical Integration of Differential Equations of Second Order Without Explicit First Derivatives. J. Res. Nat. Bur. Stand. 54 (1955) 119-125.

19) R.B. Duffey and D.T.C. Porthouse, Experiments on the Cooling of High-Temperature Surfaces by Water Jets and Drops. RD/B/N 2386 (1972) 23 pp.

20) R.D. Richtmeyer and K.W. Morton, Difference Methods for Initial-Value Problems. 2nd edition (Wiley, New York, 1967) 405 pp.

21) E. Smidt (editor), Properties of Water and Steam in SI-Units, kJ, bar, 0-800 °C, 0-1000 bar. (Springer,Berlin, 1969) 205 pp.

22) R.B. Duffey and D.T.C. Porthouse, The Rewetting of Hot Surfaces by Falling Films and Bottom Flooding, RD/B/N 2530 (1973) 27 pp.

23) A.C. Merrington and E.G. Richardson, The Break-Up of Liquid Jets. Proc. Phys. Sec. (London) 59 (1947) 1-13.

24) R.S. Brodkey, The Phenomena of Fluid Motions. (Addison-Wesley, Reading, Mass., 1967) 737 pp.

25) A.W. Bennet et al., The Wetting of Hot Surfaces by Water in a Steam Environment at High Pressure. AERE-R-5146 (1966) 13 pp.

26) J.D. Parker and R.J. Grosh, Heat Transfer to a Mist Flow. ANL-6291 (1961) 245 pp.

27) S. Bertoletti et al., Heat Transfer and Pressure Drop with Steam-Water Spray. CISE-R-36 (EURAEC-153) (1961) 166 pp.

28) E.D. Fuller, J.R. Finney, and H.E. Streeter, BWR/6 Nuclear System from General Electric, a Performance Description. NEDO-10569A (1972) 52 pp.

29) D.H. Imhoff and J.L. Murray, Experimental Basis for BWR Emergency Core Cooling. Paper presented at CREST Meeting, Munich, 18-20 October 1972. 19 pp. Unpublished work.

30) J. Andersen, Sonic Phenomena, or how to save Computation Time through a Suppression of these Phenomena. RD-Memo No. 48 (1972) 17 pp. Internal report.

APPENDIX

Heat Transfer in a Spherical Droplet

In accordance with subsection 3.3.4 it is assumed that the temperature at a steam-liquid interface will be the saturation temperature. A further assumption is that if a droplet with the temperature T_d is introduced in a steam atmosphere, the saturation temperature at the surface will immediately be established. This is the problem to be solved.

Subtracting T_d from all temperatures we have

$$\rho c \frac{\partial T}{\partial t} = k \left\{ \frac{\partial^2 T}{\partial r^2} + \frac{2}{r} \frac{\partial T}{\partial r} \right\} \qquad (A.1)$$

and the boundary conditions

$$T(r, 0) = 0 \qquad \text{for } 0 \leq r < r_o \qquad (A.2)$$

$$T(r_o, t) = T'_s \qquad \text{for } 0 \leq t < \infty \qquad (A.3)$$

$$\frac{\partial T}{\partial r}\Big|_{r=0} = 0 \qquad \text{for } 0 \leq t < \infty , \qquad (A.4)$$

where

- ρ is the density,
- c the specific heat,
- T the temperature minus T_d,
- k the thermal conductivity,
- T'_s the saturation temperature minus T_d, and
- r_o the droplet radius.

Introducing

$$a = \frac{\rho c}{k} \qquad (A.5)$$

$$f(r, s) = \hat{L}\, T(r, t), \qquad (A.6)$$

where $\hat{L}$ indicates the Laplace transformation, we obtain using (A.1) and (A.2)

$$\frac{\partial^2 f}{\partial r^2} + \frac{2}{r} \frac{\partial f}{\partial r} - asf = 0, \qquad (A.7)$$

which has the solution

$$f(r, s) = \frac{1}{r} \left\{ C_1(s) e^{-r\sqrt{as}} + C_2(s) e^{r\sqrt{as}} \right\} , \qquad (A.8)$$

where C_1 and C_2 are arbitrary functions in s.

Using the conditions (A.3) and (A.4) we obtain

$$f(r, s) = \frac{r_o T'_s \sinh(r\sqrt{as})}{r\, s \sinh(r_o\sqrt{as})} . \qquad (A.9)$$

(A.9) has the poles

$$s_n = -\frac{1}{a}\left(\frac{\pi}{r_o} n\right)^2 , \qquad n = 0, 1, 2, \ldots . \qquad (A.10)$$

and the residuum

$$res_n = \begin{cases} T'_s & \text{for } n = 0 \\ T'_s \dfrac{2 r_o \sin\left(\frac{r}{r_o} n\pi\right)}{r n \pi (-1)^n} & \text{for } n = 1, 2, 3, \ldots . \end{cases} \qquad (A.11)$$

Using Heaviside's expansion theorem we obtain

$$T(r, t) = T'_s \left\{ 1 + \frac{r_o}{r} \sum_{n=1}^{\infty} \left(\frac{2\sin\left(\frac{r}{r_o} n\pi\right)}{n\pi(-1)^n} e^{-\frac{1}{a}\left(\frac{\pi}{r_o} n\right)^2 t} \right) \right\} , \qquad (A.12)$$

and it can easily be shown that the boundary conditions (A.2), (A.3), and (A.4) are fulfilled. Consequently (A.12) represents the correct solution to the problem.

The heat transfer Q(t) to the surface is given by

$$Q(t) = 4\pi r_o^2 k \left.\frac{\partial T}{\partial r}\right|_{r = r_o}$$

$$= 8\pi r_o k T_s' \sum_{n=1}^{\infty} e^{-\frac{1}{a}(\frac{\pi}{r_o} n)^2 t} . \qquad \text{(A.13)}$$

For $t \ll a\,(\frac{r_o}{\pi})^2$ (A.13) becomes

$$Q(t) \approx 4 r_o k T_s' \sqrt{\frac{a\pi}{t}} , \qquad \text{(A.14)}$$

and for $t \gg a(\frac{r_o}{\pi})^2$ only the first term in the sum is important, and (A.13) becomes

$$Q(t) \approx 8\pi r_o k T_s' e^{-\frac{1}{a}(\frac{\pi}{r_o})^2 t} . \qquad \text{(A.15)}$$

From (A.15) it is seen that the droplet for large t will have a time constant of

$$\tau = a\,(\frac{r_o}{\pi})^2 . \qquad \text{(A.16)}$$

For a droplet radius of 10^{-3}m $\tau \approx 0.6$ seconds.

Under the assumption that the droplet has a time constant given by (A.16), the heat transfer to the surface can be expressed by a constant factor h, and (A.1) reduces to

$$\frac{4}{3}\pi r_o^3 \rho c \frac{\partial T_m}{\partial t} = 4\pi r_o^2 h T_m , \qquad \text{(A.17)}$$

where

T_m is the difference between the surface temperature and the mean temperature of the droplet. It should be noted that $T_m \neq T_s'$.

Combining (A.16) and (A.17) we obtain

$$h = \frac{k}{3}\frac{\pi^2}{r_o} . \qquad \text{(A.18)}$$

ISBN 87 550 0222 6